Biochem. J. (2012) **446**, 135–148 (Printed in Great Britain) doi:10.1042/BJ20120307

Intestinal peptidases form functional complexes with the neutral amino acid transporter B^0AT1

Stephen J. FAIRWEATHER*, Angelika BRÖER*, Megan L. O'MARA† and Stefan BRÖER*[1]

*Research School of Biology, Australian National University, Canberra, ACT 0200, Australia, and †School of Chemistry and Molecular Biosciences, University of Queensland, Brisbane, QLD 4072, Australia

The brush-border membrane of the small intestine and kidney proximal tubule are the major sites for the absorption and re-absorption of nutrients in the body respectively. Transport of amino acids is mediated through the action of numerous secondary active transporters. In the mouse, neutral amino acids are transported by B^0AT1 [broad neutral (^{0}) amino acid transporter 1; SLC6A19 (solute carrier family 6 member 19)] in the intestine and by B^0AT1 and B^0AT3 (SLC6A18) in the kidney. Immunoprecipitation and Blue native electrophoresis of intestinal brush-border membrane proteins revealed that B^0AT1 forms complexes with two peptidases, APN (aminopeptidase N/CD13) and ACE2 (angiotensin-converting enzyme 2). Physiological characterization of B^0AT1 expressed together with these peptidases in *Xenopus laevis* oocytes revealed that APN increased the substrate affinity of the transporter up to 2.5-fold and also increased its surface expression (V_{max}). Peptide competition experiments, *in silico* modelling and site-directed mutagenesis of APN suggest that the catalytic site of the peptidase is involved in the observed changes of B^0AT1 apparent substrate affinity, possibly by increasing the local substrate concentration. These results provide evidence for the existence of B^0AT1-containing digestive complexes in the brush-border membrane, interacting differentially with various peptidases, and responding to the dynamic needs of nutrient absorption in the intestine and kidney.

Key words: aminopeptidase N, angiotensin-converting enzyme 2 (ACE2), broad neutral (^{0}) amino acid transporter 1 (B^0AT1), brush-border membrane, nutrient absorption, protein complex.

INTRODUCTION

The mammalian small intestine is characterized by an epithelium forming a continuous layer of enterocytes facing the luminal cavity of the gut. The apical (brush-border) membrane of this epithelium functions as a highly specialized surface for the digestion and absorption of nutrients following the intake of food. This specialization is apparent in a series of large and small invaginations of the intestine formed by villi and microvilli, which serve to greatly increase the absorptive surface area of the brush-border for the efficient digestion and absorption of dietary nutrients [1,2]. Of particular interest is the effective absorption of dietary protein.

The digestion of proteins occurs primarily in the small intestine, where proteins are hydrolysed into small peptides (2–10 amino acids long) by intestinal proteases. Subsequent digestion occurs via the membrane-bound brush-border peptidases, which further hydrolyse small oligopeptides to produce di-/tri-peptides and single amino acids [3,4]. These digestion end-products then become substrates of amino acid and peptide transporters in the brush-border membrane [4]. Brush-border peptidases are also present in the kidney and in other tissues outside these two organs, where they mediate the hydrolysis of peptide hormones, act as cell-surface receptors and as inducers of intracellular signalling pathways [3]. The absorption of amino acids is mediated by a set of secondary active transporters, which have been characterized over the years (reviewed in [6]). The primary mediator for absorption of neutral amino acids, and hence many essential amino acids, across the apical membrane of the small intestine is the Na^+-dependent transporter B^0AT1 [broad neutral (^{0}) amino acid transporter 1; SLC6A19 (solute carrier family 6 member 19)] [5,6]. Mutations in B^0AT1 cause Hartnup disorder, a symptomatically heterogeneous disease characterized by high levels of fecal amino acids and renal aminoaciduria [7,8].

Protein digestion has generally been viewed as being carried out by a number of individual enzymes and transporters functioning independently [9]. However, the discovery that the carboxypeptidase ACE2 (angiotensin-converting enzyme 2) is required for the trafficking of B^0AT1 *in vitro* and *in vivo* in the intestine has led us to re-evaluate this view [10,11]. In the kidney, B^0AT1 is trafficked to the plasma membrane by collectrin, a non-peptidase homologue of ACE2 [12]. These discoveries raise the possibility that a close association between brush-border peptidases and neutral amino acid transporters may be a widespread phenomenon on the absorptive epithelial surfaces. Evidence for this was provided by an earlier observation that removal of another brush-border hydrolase, APN (aminopeptidase N) from bovine renal BBMVs (brush-border membrane vesicles) by papain treatment, significantly reduced Na^+-dependent alanine transport [13]. Moreover, an antibody raised against a partially purified Na^+-dependent alanine transporter was found to recognise APN, suggesting a close proximity of both proteins. Further characterization of these vesicles demonstrated that both the V_{max} and apparent K_m for the uptake of various neutral amino acids were affected by the removal of APN. However, the study used the cysteine protease papain to remove APN from the BBMVs, a rather non-specific treatment likely to remove extracellular domains from a variety of membrane proteins. In

Abbreviations used: ACE2, angiotensin-converting enzyme 2; APN, aminopeptidase N; B^0AT, broad neutral (^{0}) amino acid transporter; BBMV, brush-border membrane vesicle; DTT, dithiothreitol; eGFP, enhanced green fluorescent protein; FBS, fetal bovine serum; GFP, green fluorescent protein; HEK, human embryonic kidney; LAP, leucine aminopeptidase; NCBI, National Centre for Biotechnology Information; RMSD, root mean square deviation; SLC, solute carrier; sulfo-NHS-LC-biotin, sulfosuccinimidyl 6′-(biotinamido) hexanoate.

[1] To whom correspondence should be addressed (email stefan.broer@anu.edu.au).

addition, the molecular correlate of neutral amino transport in these vesicles was unknown at the time.

APN, the most abundant peptidase in the mammalian small intestine [14], is a zinc metalloprotease that homodimerizes *in vivo* and hydrolyses N-terminal amino acids at the brush-border membrane, except when a proline lies adjacent to the *N*-terminal amino acid [3]. The active site of APN defines its specificity for N-terminal amino acid residues. All aminopeptidase family members belong to the gluzincin metalloprotease family, with two consensus zinc-binding sequences, **H**EXX**H** and BX**L**X**E** (zinc-binding residues are indicated in bold, B indicates a bulky side-chain residue and X denotes any residue) [15]. In addition, a third consensus site **G**X**M**E**N** is an exopeptidase substrate-binding sequence also common to all aminopeptidases. The hypothetical structure of human APN has a seven-domain topology. The first three domains form the *N*-terminal of the protein, comprising a small cytoplasmic tail, a single transmembrane α-helix and an extracellular anchoring domain. This anchoring domain links to the remaining four extracellular domains responsible for catalytic activity [15,16]. APN has a broad specificity for neutral amino acids in the order Ala>Phe>Tyr>Leu, overlapping with the substrate preference of B^0AT1 (Leu>Gln>Ala>Phe) [17,18].

Protein complexes containing APN and other brush-border peptide hydrolases have been isolated from intestinal brush-border membranes using Blue native electrophoresis [19], but these did not seem to contain membrane transporters. There is also evidence of a role for intestinal microvillar micro-domains or lipid rafts in the sorting and trafficking of some apical proteins [20–24]. However, the physiological significance of any of these protein complexes at the brush border is still largely unknown.

In the present study, we demonstrate for the first time that the main neutral amino acid transporter of the mammalian small intestine B^0AT1 forms complexes with the peptidase APN in addition to its known interaction with ACE2. We demonstrate that APN alters the transporter's kinetic parameters. Finally, we investigate the possible mechanisms by which these functional alterations of the transporter's kinetic properties might occur.

EXPERIMENTAL

Preparation and characterization of mouse intestinal BBMVs

Male or female C57BL/6J mice (12–24 weeks old) were killed by cervical dislocation and the entire small intestine from the pyloric sphincter to the ileocaecal sphincter was removed. All animal handling was approved by the Animal Experimental Ethics Committee and performed in accordance with the institutional guidelines at the Australian National University (Protocol F.BMB.35.07). BBMVs were isolated and enriched from mouse intestinal epithelial cells using a protocol adapted from Biber et al. [25]. Total protein content and enrichment of proteins from homogenized intestinal mucosa was measured using Bradford protein and alkaline phosphatase assays. Preparations gave a total protein concentration of 4–15 mg/ml for intestinal BBMVs with a typical enrichment of between 10- to 15-fold for brush-border-specific proteins over intestinal homogenates.

Quantification and functional activity of APN were measured using colorimetric assays at 25 °C with either 6.5 mM L-alanine-4-nitroanilide or L-leucine-4-nitroanilide substrates in assay buffer (262 mM Tris/HCl and 262 mM NaCl, pH 7.8). The A_{405} of the liberated 4-nitroaniline was quantified spectrophotometrically, with a ε_{405} of 9951 $M^{-1}\cdot cm^{-1}$ [26,27]. Specific activity was converted to $\mu mol\cdot min^{-1}\cdot \mu g$ of $protein^{-1}$, and the quantity of APN as a percentage of total BBMV protein was calculated using the relative activity of purified APN type IV-S from porcine kidney microsomes (Sigma–Aldrich). Proteins in BBMVs were detected by Western blotting.

Blue native PAGE

Blue native gel electrophoresis experiments were adapted from Schagger and Von Jagow [28]. Briefly, 40 μg of BBMVs (1 μg/μl) was solubilized for 30 min in detergent buffer [20 mM Bis-Tris, pH 7, 50 mM NaCl, 10 % (v/v) glycerol and 1 mM DTT (dithiothreitol)] containing either digitonin or Triton X-100 at 0.5 or 1 % respectively. Samples were centrifuged at 16 000 ***g*** at 4 °C for 5 min and the supernatant was transferred into a new microfuge tube. Non-solubilized pellets were retained to determine the efficiency of the solubilization process by measuring the remaining protein concentration at $\lambda = 280$ nm and /or by Western blotting. Blue native loading dye was added to samples to give a final concentration of 0.5 % Coomassie Brilliant Blue G-250 (50 mM ε-amino n-caproic acid and 10 mM Bis-Tris, pH 7). Samples were run on a discontinuous gel buffered system, with a 4–16 % gradient gel and 4 % stacking gel (gel buffer: 66 mM ε-amino n-caproic acid and 50 mM Bis-Tris, pH 7.0). A PROTEAN-3™ gel electrophoresis system (Bio-Rad Laboratories) was used with cathode chamber buffer containing 50 mM tricine, 15 mM Bis-Tris (untitrated) and 0.2 % Coomassie Brilliant Blue G-250, and anode chamber buffer containing 50 mM Bis-Tris, pH 7.0. Gels were run at 4 °C for 16 h at 100 V. The Coomassie Blue-containing cathode buffer was changed to a buffer without Coomassie Blue approximately 4 h into the run to avoid the transfer of excess dye, which inhibits antibody detection. Transfer on to methanol-activated PVDF membranes (GE Healthcare) was completed at $\leqslant$20 V with a current density of 1 mA/cm^2 for 2 h on a Hoefer SemiPhor™ semi-dry transfer system. Membranes were stained to visualize marker proteins [50 % (v/v) methanol, 7 % (v/v) glacial acetic acid and 0.1 % Coomassie Brilliant Blue G-250] and de-stained again for protein detection [90 % (v/v) methanol and 10 % (v/v) glacial acetic acid]. Thyroglobulin (669 kDa), ferritin type 1 from horse spleen (440 kDa) and BSA (134 and 67 kDa) (all from Sigma–Aldrich), were used as molecular mass markers. These marker proteins were used to create a standard curve for each of the three repeated Blue native experiments. The molecular mass calculations were then derived from each standard curve and the means $\pm$ S.D. of each complex are represented in Table 1. Proteins were detected using Western blotting.

Table 1 Molecular masses of protein complexes isolated from the murine intestinal brush-border

Protein complexes were identified using 4–16 % non-continuous Blue native PAGE (see Figure 1A). The protein standards, thyroglobulin (669 kDa), ferritin (440 kDa) and BSA (134 kDa and 69 kDa), were used to create a standard curve for calculating mean molecular mass (M.M.) $\pm$ S.D. ($n = 3$).

Complex	Solubilization conditions	Proteins detected	M.M. (kDa $\pm$ S.D.)
1	Digitonin 0.5 %/1 % (w/v)	B^0AT1, ACE2	611 $\pm$ 11
2	Digitonin 0.5 %/1 % (w/v)	B^0AT1, ACE2	558 $\pm$ 5
3	All conditions	B^0AT1, ACE2, APN	488 $\pm$ 3
4	Digitonin 0.5 %/1 % (w/v)	ACE2	376 $\pm$ 6
5	Triton X-100 0.5 %/1 % (v/v)	APN	195 $\pm$ 3
6	Triton X-100 0.5 %/1 % (v/v)	B^0AT1	155 $\pm$ 39 to 45 $\pm$ 18
7	Triton X-100 0.5 %/1 % (v/v)	ACE2	63 $\pm$ 8

Preparation of detergent-resistant membranes

Detergent-resistant membranes/lipid rafts were prepared as outlined by Danielsen [29], Danielsen and van Deurs [30] and Waugh and Hsuan [31]. Briefly, BBMVs at 1–2 mg/ml were treated for 30 min at 0–4 °C in 2 ml of 1 % (v/v) Triton X-100 buffer [150 mM NaCl, 25 mM Hepes, pH 6.5, and 1 % (v/v) Triton X-100]. The complete membrane extract was then diluted with an equivalent volume of 80 % (w/v) sucrose dissolved in the same buffer to create a 40 % (w/v) sucrose gradient bed. The mixture was carefully overlaid with a 5–30 % (w/v) linear sucrose gradient and then centrifuged at 3 °C at 212 000 ***g*** (68 000 rev./min) for 24 h in a Beckmann SW41Ti swing-out rotor (Beckmann-Coulter). Sucrose gradient fractions were collected from the bottom of the centrifugation tube in 0.8 ml fractions. All fractions were stored at − 80 °C and analysed by SDS/PAGE for the presence of specific proteins.

Co-immunoprecipitation of membrane proteins

For co-immunoprecipitations, 150–300 μg of BBMVs were solubilized for 1 h at 1 μg/μl in co-immunoprecipitation buffer [20 mM Tris, pH 7.4, 150 mM NaCl, 5 mM MgCl and 1 % (v/v) Triton X-100] containing the Complete™ EDTA-free protease inhibitor cocktail (Roche Diagnostics). The lysate was then cleared by centrifugation at 15 000 ***g*** and 4 °C for 20 min and transferred into a new reaction tube. The cleared lysate was incubated overnight at 4 °C on rotation with 2 μl of primary antibody against either B^0AT1 (custom generated by Pineda Antibody Service) or APN (Epitomics) and Protein-A-conjugated agarose beads (Pierce Biotechnology). Samples were subsequently washed five times with the co-immunopreciptiation buffer at 4 °C followed by a 30 s centrifugation at 3000 ***g*** each time. Samples were prepared for SDS/PAGE in 10× Laemmli sample buffer containing DTT (Invitrogen). Samples (20 μl) were run on 4–12 % Bis-Tris pre-cast gels (Invitrogen) in Mes (50 mM Mes, 50 mM Tris, 0.1 % SDS and 1 mM EDTA, pH 7.3) or Mops (50 mM Mops, 50 mM Tris, 0.1 % SDS and 1 mM EDTA, pH 7.7) buffer, and transferred using the Invitrogen iBlot™ dry transfer system on to nitrocellulose membranes.

Membrane stripping and Western blotting

Both nitrocellulose and PVDF membranes were blocked overnight in 10 % (w/v) non-fat dried skimmed milk powder/PBS-Tween 20 (0.1 %) solution at 23 °C. Blots were incubated in the blocking solution for 2 h with the following primary antibodies at the indicated dilutions: anti-(mouse B^0AT1) (1:3000) (Pineda Antibody Service), anti-(human APN) (1:2000) (Epitomics), anti-(mouse ACE2) (1:4000) (Abcam), anti-(mouse collectrin) (1:2000) (Enzo Life Science), anti-(mouse β-actin) (1:2000) (Abcam), anti-(human Na^+/K^+-ATPase) (1:25 000) (Abcam), or anti-(human caveolin-1) (1:2000) (Abcam). Goat anti-rabbit (Jackson ImmunoResearch) or sheep anti-mouse (GE Healthcare) HRP (horseradish peroxidase)-conjugated antibodies were used for secondary detection. Where indicated, Western blots were quantified on the basis of pixel density using ImageJ software v1.43u (National Institutes of Health).

Nitrocellulose and PVDF membranes were stripped of antibodies and milk powder by incubation in a stripping buffer [100 mM 2-mercaptoethanol, 2 % (w/v) SDS and 62.5 mM Tris/HCl, pH 6.7] and heated at 60 °C for 30 mins. To remove 2-mercaptoethanol, membranes were then washed three times for 10 min in a suitable volume of PBS-Tween 20 (0.1 %).

Tissue samples were surgically removed from a single 12–24-week-old female C57BL/6J mouse and homogenized in T-PER homogenization reagent (Thermo Fisher Scientific) at a concentration of 50 mg/ml. A Bradford protein quantification assay was conducted prior to Western blotting to standardize the amount of total protein loaded per sample.

cDNA cloning and plasmid generation

Murine B^0AT1, ACE2 or collectrin cDNAs in pGem-He-Juel were used as described previously [11]. Murine APN was amplified from mouse intestinal cDNA using the sense primer 5′-CGCCACCATGGCCAAGGGGTTCTACAT-3′ and antisense primer 5′-CAGGAACTAACTGCTGTTCTCTGTGAA-3′. Following amplification, the APN PCR product was inserted into pZero Blunt (Invitrogen), the insert was then excised using EcoRI and ligated into pGem-He-Juel. The integrity and orientation of the cloned cDNA was verified by sequencing (Australian National University, Biomolecular Resource Facility, Canberra, Australia). All genes, cRNA and proteins in the present paper originated from *Mus musculus* unless otherwise indicated.

Expression of transporters in *Xenopus laevis* oocytes

Isolation and preparation of *X. laevis* oocytes for injecting of cRNA and expression of plasma-membrane proteins has been described previously [32]. Oocytes were maintained in OR^{2+} buffer (82.5 mM NaCl, 2.5 mM KCl, 1 mM $MgCl_2$, 1 mM Na_2HPO_4, 5 mM Hepes, 1 mM $CaCl_2$ and 50 μg/ml gentamycin, pH 7.8) at 18 °C. The B^0AT1, APN, ACE2 and Collectrin constructs cloned into pGem-He-Juel were linearized using SalI or NotI restriction endonucleases, and *in vitro* transcribed using the T7 mMessage mMachine Kit (Ambion) as described previously [11,32]. APN wild-type or site-directed mutant cRNA (15 ng per oocyte) was injected into the oocyte, the injection amount of all other cRNAs having been previously optimized [11,17]. Oocytes were used 4–6 days post-injection unless otherwise indicated. All electrophysiology and uptake experiments were conducted in ND96 buffer (96 mM NaCl, 2 mM KCl, 1 mM $MgCl_2$, 1.8 mM $CaCl_2$ and 5 mM Hepes, titrated with NaOH to pH 7.4) unless otherwise stated.

Electrophysiological recordings and flux measurements

Electrical recordings of amino-acid-induced currents and uptake of radiolabelled amino acids were performed as described previously [17,32]. In all electrophysiology experiments where substrate was applied multiple times, the results were normalized to a reference superfusion of 10 mM L-leucine for B^0AT1 made at regular intervals. This was done to compensate for any run-down effect of B^0AT1-mediated transport. The function of APN and its site-directed mutants was tested using the tetrapeptide NH_2-Leu-Ser-Lys-Leu-COOH (Sigma–Aldrich) or NH_2-Leu-Leu-Leu-COOH (Bachem). The tetrapeptide and all single amino acid substrates were titrated to pH 7.4 before use. For experiments where the di-peptide analogue bestatin hydrochloride (Sigma–Aldrich) was used, oocytes were pre-incubated for 1 min in 70 μM bestatin before a mixed solution of 100 μM [^{14}C]leucine and 70 μM bestatin was added. This concentration represented 10× the inhibition constant (K_i) for *Escherichia coli* APN [33], and was used to ensure maximum competition for murine APN hydrolytic activity.

Surface biotinylation of *X. laevis* oocytes

Surface biotinylation of *X. laevis* oocytes was performed as described previously [32]. Following incubation at 18 °C for 5 days post-injection of cRNA, 15 oocytes were selected and washed three times in ice-cold PBS buffer (137 mM NaCl, 2.7 mM KCl and 5 mM Na_2HPO_4, pH 8.0). Oocytes were incubated in 0.5 mg/ml of EZ-Link™ sulfo-NHS-LC-biotin [sulfosuccinimidyl 6′-(biotinamido) hexanoate; Thermo Fisher Scientific] dissolved in PBS (pH 8.0) for 45 mins at room temperature (21 °C) and then washed three times in ice-cold PBS buffer. The plasma membranes were solubilized on ice in oocyte lysis buffer [150 mM NaCl, 20 mM Tris/HCl and 1 % (v/v) Triton X-100, pH 7.6] for 2 h with occasional gentle inversion and then incubated at 4 °C in 50 μl of streptavadin-coated agarose beads (Thermo Fisher Scientific). Samples were set on slow rotation overnight. Beads were then washed four times with oocyte lysis buffer with a 10 min centrifugation at 16000 ***g*** following each wash. Samples were prepared for SDS/PAGE as described previously.

Cell culture

HEK (human embryonic kidney)-293 cells were cultured in RPMI 1640 cell growth medium (John Curtain Medical Research School, Australian National University, Canberra, Australia) containing 10 % (v/v) FBS (fetal bovine serum) and 2 mM glutamine. Incubation occurred at 37 °C in a 95 % air/5 % CO_2 incubator. Cells were passaged at 75–80 % confluency by treatment with 0.25 % trypsin/EDTA (Invitrogen) until the solution became opaque, indicating detachment of the cells from the flask surface. Trypsin activity was stopped by the addition of medium containing FBS. Cells were centrifuged at 1500 ***g*** for 5 min to pellet, the media was aspirated and the cells were resuspended in RPMI 1640 medium [containing 5 % (v/v) FBS and 2 mM glutamine] before seeding into a fresh culture flask.

Co-localization of membrane proteins using the Venus fly trap

The original Venus fly trap vectors encode antiparallel leucine-zipper motifs, with each zipper fused to one half of GFP (green fluorescent protein) from *Aequorea victoria* in pcDNA3.1 Zeo(+) [34]. Two vectors, Venus[1]-zip and zip-Venus[1], contain GFP residues 1–157, another two, Venus[2]-zip and zip-Venus[2], contain GFP residues 158–238. Murine B^0AT1 was sub-cloned into Venus[2]-zip/pcDNA3.1Zeo(+) and Venus[1]-zip/pcDNA3.1Zeo(+) from pGem-He-Juel using the sense primer 5′-ATATCCGGAATGGTGAGGCTTGTGCTGCC-3′ and the antisense primer 5′-CCCTCTAGATCAGTTCTTAAGGTC-CCCAT-3′ to generate Venus2-B^0AT1/pcDNA3.1Zeo(+) and Venus1-B^0AT1/pcDNA3.1Zeo(+) with GFP 158–238 or GFP 1–157 at the N-terminus of B^0AT1 respectively. Murine B^0AT1 was also sub-cloned into zip-Venus[2]/pcDNA3.1Zeo(+) using the sense primer 5′-TTAAGCGGCCGCATGGTGAGGCTTGTGCT-GCC-3′ and the antisense primer 5′-GCCACCATCGATGTTC-TTAAGGTCCCCATT-3′ to generate B^0AT1-Venus2/pcDNA3. 1Zeo(+) with GFP 158–238 at the C-terminus of B^0AT1. Murine APN was sub-cloned into Venus[1]-zip/pcDNA3.1Zeo(+) from pGem-He-Juel using the sense primer 5′-AGCGATATC-AATGGCCAAGGGGTTCTAC-3′ and the antisense primer 5′-CCCTCTAGACTAACTGCTGTTCTCTGT-3′ to generate Venus1-APN/pcDNA3. 1Zeo(+) with GFP 1–157 at the N-terminus of APN. Both B^0AT1 and APN were sub-cloned to allow for possible interaction between intracellular termini: the C-terminus (B^0AT1-Venus2) and N-terminus (Venus2-B^0AT1) of B^0AT1 or N-terminus (Venus1-APN) only in the case of APN. The assay was conducted by seeding 75–80 % confluent HEK-293 cells into 0.7 cm^2 8-well covered Millicell EZ™ microscope slides (Millipore). The cells were incubated for 24–48 h in RPMI 1640 medium [with 10 % (v/v) FBS and 2 mM glutamine, in 5 % CO_2 at 37 °C] until they had reached >90 % confluency. Transfection of Venus fly trap constructs was then carried out using Lipofectamine™ 2000 reagent (Invitrogen) with 1.6 μg of total DNA per well. Transfected cells were incubated for 48 h before the medium was aspirated and mounted with ProLong anti-fade Gold™ (Invitrogen). Slides were cured for 24 h and then sealed with epoxy resin. The eGFP (enhanced GFP) fluorescence was visualized at λ_{ex} of 485 nm from an argon laser, with emission recorded at 492–550 nm. All images were captured using the following settings: bright-field gain, 250 HV; fluorescent light gain, 600 HV; scan speed, 400 Hz; and 1024×1024×1024 pixel resolution. In images where cellular outlines were visualized, the bright-field gain was increased to between 280 HV and 330 HV. All digital images were taken under identical conditions using the LAS AF software visualized using the Leica SP5 confocal system. HEK-293 cells were visualized using a ×63 oil objective.

Sequence alignments and homology model of APN

Protein sequences used for alignment were obtained from the ExPASy proteomics servers Uniprot Knowledgebase database (http://au.expasy.org/). Identification of proteins homologous to mouse APN was conducted using the NCBI (National Centre for Biotechnology Information)'s BlastP protein sequence search and alignment tool (http://blast.ncbi.nlm.nih.gov/Blast.cgi). Multiple searches against mouse APN were aligned using NCBI COBALT (http://www.ncbi.nlm.nih.gov/tools/cobalt/cobalt.cgi?CMD=Web).

The murine APN homology model was generated using the HHpred comparison tool from the Bioinformatics Toolkit website of the Max-Planck Institute for Development Biology (http://toolkit.tuebingen.mpg.de/hhpred). After checking that the results of the HHpred search contained the same reference proteins against which the sequence alignments had been conducted, the target sequences were matched to the reference PDB structural co-ordinates in order to create the homology model. The protein structure of murine APN was visualized using PyMol 9.9 (DeLano Scientific). *In silico* verification of the murine APN model was conducted as previously outlined for homology structures [35]. Primary checking was conducted using WHATIF [36] and PROCHECK [37], which verify local factors, such as dihedral angle distribution, backbone conformation, bond lengths and backbone packing. The backbone RMSD (root mean square deviation) between *E. coli* LAP (leucine aminopeptidase) and murine APN was 0.68 Å (1 Å = 0.1 nm). Analysis of the Ramachandran plot in Swiss-PdbViewer (http://spdbv.vital-it.ch/) showed >95 % of dihedral angles in the allowable regions.

Site-directed mutagenesis

Single point mutations were introduced into the APN cDNA using the QuickChange® II Site-Directed Mutagenesis Kit (Stratagene). Briefly, complementary primers, containing the desired mutation flanked by 15 nucleotides corresponding to the APN cDNA sequence, were used to amplify the complete cDNA-containing pGem-He-Juel vector. The following oligo-nucleotide primers were used to introduce the indicated mutation

in APN (mutated nucleotides are in bold): E354A sense primer, 5′-ACGCTGGAGCCATGG**C**GAACTGGGGTCTGGT-3′ and antisense primer, 5′-ACCAGACCCCAGTTC**G**CCATGGCTCCAG-CGT-3′; E388A sense primer, 5′-CTGTGATTGCTCACG**C**G-CTGGCCCATCAGTG-3′ and antisense primer, 5′-CACTG-ATGGGCCAGC**G**CGTGAGCAATCACAG-3′; E410A sense primer, 5′-ATCTGTGGCTGAACG**C**GGGCTTTGCCTCCTA-3′ and antisense primer, 5′-TAGGAGGCAAAGCCC**G**CGTTCAG-CCACAGAT-3′; and Y476F sense primer, 5′-TTGACAGCAT-CACCT**T**CAGCAAGGGAGCCTC-3′ and antisense primer, 5′-GAGGCTCCCTTGCTG**A**AGGTGATGCTGTCAA-3′. All mutations were subsequently verified by sequencing (Australian National University, Biomolecular Resource Facility).

Calculations, statistics and data analysis

For all electrophysiological recordings, results were averaged for 6–8 oocytes, unless otherwise indicated. Incubation of non-injected *X. laevis* oocytes with amino acids typically induced only small endogenous currents, which amounted to less than 5 % of the current generated by heterologously expressed transporters. These remained uncorrected. Baseline corrections and analysis of current tracings were conducted using the Clampfit 8.2 or 10.2 software (MDS Analytical Technologies). For flux experiments using radiolabelled amino acids, the transport activity was averaged over 8–12 oocytes, unless otherwise indicated, and the activity of non-injected oocytes was subtracted.

The kinetic constants of apparent K_m and V_{max} were derived by fitting the semi-hyperbolic Michaelis–Menten equation $v = V_{max}S/(K_m + S)$ to the experimental electrophysiological data points. The data was then plotted and fitted to the Eadie–Hofstee equation $v = v/S(-K_m) + V_{max}$ for visualization. All curve fitting and determination of kinetic parameters were performed using Origin 7.0 or 8.0 software (OriginLab). To convert I_{max} values into transport rates (V_{max}), a conversion rate of 37 pmol/h = 1 nA was used.

Unless otherwise stated, all data are presented as means ± S.D. Significance was evaluated using the Student's *t* test in the case that only two experimental conditions were tested. In cases where more than three experimental conditions were tested, either one-way or two-way ANOVA was used to test for overall significance, with the Bonferroni post-hoc test to determine significance between pairs of conditions within the larger experiment. A Pearson's correlation test was used to determine the linear dependence between peptide-induced catalytic activity of APN mutants and the apparent K_m of associated B^0AT1-mediated leucine transport. All Figures are a single representative example of at least three repeats conducted for all experiments unless otherwise stated.

RESULTS

Evidence for protein complexes in the intestinal brush-border membrane

In agreement with earlier findings, B^0AT1, ACE2 and APN were significantly enriched in BBMVs compared with homogenized intestinal mucosa (Supplementary Figure S1A at http://www.BiochemJ.org/bj/446/bj4460135add.htm). The renal trafficking facilitator collectrin was not detected in BBMVs, but was detected in the intestinal mucosa homogenates, indicating expression outside the apical membrane. APN function was demonstrated using the peptidomimetic colorimetric substrates L-leucine-4-nitroanilide or L-alanine-4-nitroanilide (Supplementary Figure S1B). APN was estimated to comprise approximately 2.7 ± 0.3 % of total protein in BBMVs and 0.5 ± 0.1 % of total protein from the intestinal homogenate on the basis of relative enzymatic activity using a purified kidney porcine APN as a standard (Sigma–Aldrich).

Solubilization of BBMV membrane proteins with two different detergents, followed by Blue native gel electrophoresis, revealed the presence of large protein complexes containing B^0AT1, APN and/or ACE2 (Figure 1A). An overview of the complexes and their protein content is presented in Table 1. Solubilization in digitonin (0.5 % or 1 %, w/v) resulted in two large complexes (1 and 2) containing B^0AT1 and ACE2 at 611 ± 11 kDa and 558 ± 5 kDa respectively. A slightly smaller complex (3) at 488 ± 3 kDa appeared to contain all three proteins and a smaller complex containing ACE2 only was detected at 376 ± 6 kDa (4). The presence of the protein monomer for APN was confirmed by solubilization in the non-ionic detergent Triton X-100 (5). Also, when solubilized with Trition X-100, B^0AT1 was detected in a smear ranging from 155 ± 39 kDa to 45 ± 18 kDa (6), and ACE2 at 63 ± 8 kDa (7). The absence of β-actin in every sample confirmed the solubilization of isolated lipid-soluble complexes exclusively (results not shown). The size of the complexes suggest that B^0AT1, ACE2 and APN could interact with a variety of brush-border membrane proteins (see the Discussion section).

Detection of membrane proteins in complexes of the same molecular mass provides evidence for protein–protein interaction, but the similarity of the molecular mass could be incidental. To provide further evidence, co-immunoprecipitation was used. Following solubilization of BBMVs, pull-down of B^0AT1 revealed co-immunoprecipitation of APN and, vice versa, the pull-down of APN revealed the co-immunoprecipitation of B^0AT1 (Figure 1B).

To examine whether the isolated complexes were contiguous with detergent-resistant membrane micro-domains, BBMVs were treated with Triton X-100 at 0–4 °C and the suspension was separated by density equilibrium centrifugation on a linear sucrose gradient. All three proteins co-segregated to the lipid-containing opaque fractions 7 and 8 (Supplementary Figure S2A at http://www.BiochemJ.org/bj/446/bj4460135add.htm). The majority of ACE2 and APN protein did, however, remain in the soluble protein fractions of the gradient bed (fractions 1–5), whereas a larger proportion of B^0AT1 was retained in the floating lipid-raft fractions. Interestingly, the peptidases, but not B^0AT1, also appeared in the last two sucrose gradient fractions (14–15), corresponding to the lowest density area of the sucrose gradient. Caveolin-1, a lipid-raft marker from other tissues but not intestinal epithelial cells [30], was not detected in either the soluble or detergent-resistant fraction. To confirm the specificity of the rabbit anti-(human caveolin-1) antibody in detecting murine caveolin-1, it was tested against several mouse tissue samples (Supplementary Figure S2B). Caveolin-1 was strongly detected in mouse heart and lung tissue, faintly detected in spleen and kidney, but not detected at all in liver or intestinal tissue samples, consistent with its use as a negative control for intestinal epithelial lipid raft detection.

To further investigate the specificity of the APN–B^0AT1 interaction, we used a protein complementation assay in which both APN and B^0AT1 were fused to halves of the eGFP protein (Figure 2). Venus1 represents eGFP residues 1–157 and was fused to the intracellular N-terminus of APN (Venus1–APN), whereas Venus2 represents eGFP residues 158–238 fused to either the intracellular N-terminus (Venus2–B^0AT1) or C-terminus (B^0AT1–Venus2) of B^0AT1. If protein–protein interactions bring the two halves of eGFP close together, fluorescence can be observed [34]. Transfection of B^0AT1–Venus2 or Venus2–B^0AT1 with Venus1–APN constructs in HEK-293 cells resulted in a

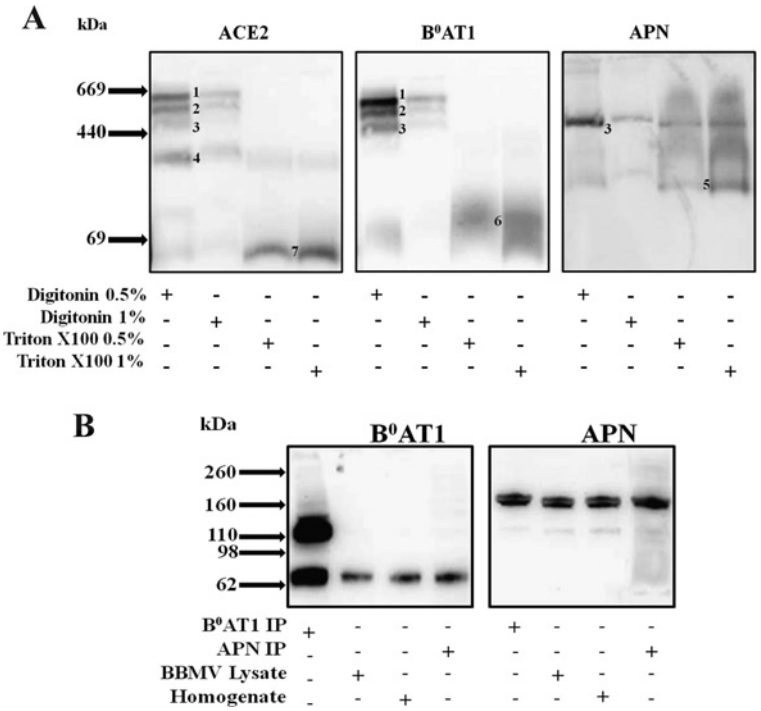

Figure 1 Isolation of intestinal brush-border protein complexes

Murine intestinal BBMVs were prepared using $MgCl_2$ precipitation and centrifugation. (**A**) BBMVs (50 μg/sample) at 1 mg/ml were solubilized in detergent buffer as indicated and mixed with Coomassie Brilliant Blue G-250 loading dye before separation. Samples were separated by Blue native PAGE. Following semi-dry transfer on to a PVDF membrane, individual proteins were detected by immunoblot analysis. The blot was stripped and re-probed for the proteins indicated, to allow a direct comparison of band positions. Protein complexes and individual proteins are numbered 1–7 (discussed in the main text). (**B**) Murine BBMVs were solubilized in co-immunoprecipitation buffer, followed by incubation with Protein A and primary antibodies against either B^0AT1 or APN. After overnight incubation of BBMV samples, the cleared lysate and intestinal homogenate were separated by SDS/PAGE. Following semi-dry transfer on to a nitrocellulose membrane, the blots were pre-stripped using stripping buffer and blocked overnight to reduce background signal. Individual proteins were then detected as indicated above the blot and visualized using immunoblot analysis. Molecular masses are indicated to the left-hand side in kDa.

significant green fluorescent signal above background, suggesting that both halves could recombine. When HEK-293 cells were co-transfected with Venus1–B^0AT1 and Venus1–APN vectors, containing the same half of the eGFP protein (residues 1–157), no fluorescence was observed. In the absence of collectrin, the kidney-specific B^0AT1-trafficking subunit (Figure 2, left-hand panel), the fluorescence induced by the Venus2–B^0AT1/Venus1–APN and B^0AT1–Venus2/Venus1–APN vector pairs was observed largely inside the cells and not at the plasma membrane. In contrast, when the same vector pairs were co-transfected with collectrin (Figure 2, right-hand panel), co-localization of B^0AT1 and APN predominated at the plasma membrane. The transfection of individual eGFP halves showed only background fluorescence (Supplementary Figure S3 at http://www.BiochemJ.org/bj/446/bj4460135add.htm).

Effects of APN on the transport kinetics of B^0AT1

Taken together, the results suggest a close association of B^0AT1, ACE2 and APN in the brush-border membrane. To investigate whether there are functional interactions between these proteins, we expressed them in *X. laevis* oocytes. As previously reported, expression of B^0AT1 in *X. laevis* oocytes resulted in a significant increase in the uptake of neutral amino acids [7,38], which was strongly stimulated further by co-expression of B^0AT1 with the carboxypeptidase ACE2 [10,11] (Figure 3A) ($P < 0.001$). Co-expression of APN with B^0AT1 resulted in a 4-fold increase in [^{14}C]leucine (100 μM) uptake over oocytes expressing only B^0AT1 ($P < 0.05$), which was not as high as that observed when B^0AT1 was co-expressed with ACE2. Functional expression of APN in oocytes was demonstrated by superfusing *X. laevis* oocytes with the tetra-peptide Leu-Ser-Lys-Leu and recording the resulting B^0AT1-mediated currents created by transport of the liberated N-terminal leucine (Figure 3B).

The increase of B^0AT1 activity following APN co-expression was confirmed through the measurement of amino-acid-induced Na^+ co-transport currents (Figure 3C). Interestingly, the increase in sodium current, measured at a substrate concentration of 10 mM, was only double that observed in oocytes expressing B^0AT1 alone. By contrast, the increase in amino acid uptake at 100 μM leucine from flux experiments showed a 4-fold increase in leucine transport in B^0AT1/APN co-expressing oocytes (Figure 3D) ($P < 0.01$ or $P < 0.001$ for 10 mM and 100 μM leucine respectively). These results raised the possibility that APN may alter the substrate affinity of B^0AT1-mediated neutral amino acid transport.

A kinetic characterization of B^0AT1 and APN co-expressing oocytes revealed that APN significantly increased the apparent substrate affinity of B^0AT1-mediated leucine transport (apparent $K_m = 0.52 \pm 0.02$ mM) ($P < 0.001$), whereas oocytes expressing B^0AT1 alone gave an apparent K_m value of 1.02 ± 0.06 mM, consistent with our previous findings (Figure 4A) [17,39]. We could also confirm our previous observation that co-expression of ACE2 does not affect the substrate affinity of B^0AT1 [11] (apparent $K_m = 1.09 \pm 0.04$ mM). These results were confirmed by analysing the transport kinetics of several of the main B^0AT1 substrates (Table 2). Leucine, glutamine and phenylalanine showed a 2- to 3-fold increase in substrate affinity in oocytes co-expressing APN.

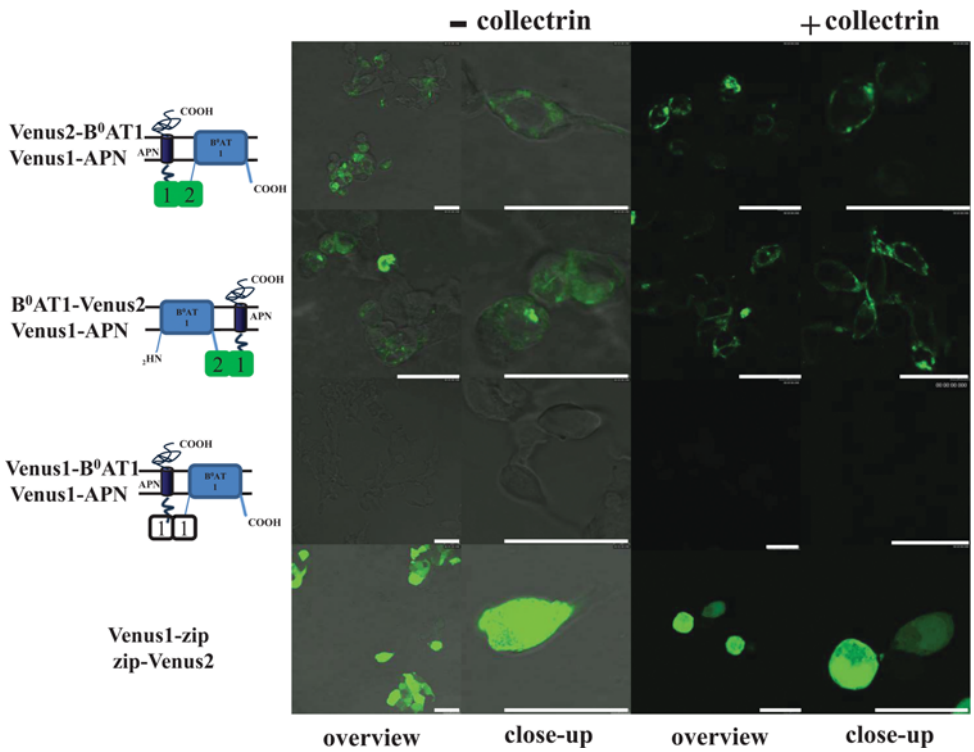

Figure 2 Co-localization of B^{0}AT1 and APN

HEK-293 cells in eight-well microscope slide dishes were transfected with plasmid DNA (constructs used are indicated on the left-hand side) when cells had achieved >90 % confluency. The eGFP fluorescence was visualized with a Leica SP5 confocal system and processed with LAS AF software. Indicated above the panels is whether or not cells were co-transfected with the pcDNA mammalian expression vector encoding the trafficking protein collectrin. The white scale bars indicate 25 μm. All images were taken at ×63 magnification.

The APN-mediated increase in B^{0}AT1 substrate affinity did not, however, account for the total ~4-fold increase in leucine transport rate observed in flux experiments at sub-K_m substrate concentration (Figures 3A and 3D). This suggested the possibility that APN may also act as a facilitator of B^{0}AT1 trafficking to the plasma membrane, similar to the role of ACE2 with B^{0}AT1 [11]. To investigate this possibility, we monitored the temporal interaction between B^{0}AT1 and APN by measuring their co-expression in oocytes over 6 days (Figure 4B). A significant increase in B^{0}AT1-mediated transport was observed at days 5 and 6 post-injection onwards ($P < 0.001$). This pattern differs to the steady increase in membrane expression observed when B^{0}AT1 and ACE2 are co-expressed [11], suggesting APN may not be a strong facilitator of B^{0}AT1 trafficking.

Quantification of trafficking using surface biotinylation indicated a 2.6 ± 0.9-fold increase of surface expression in B^{0}AT1 and APN-co-expressing oocytes compared with oocytes expressing B^{0}AT1, as exemplified in Figure 4(C). In contrast, ACE2 co-expression resulted in a 32.0 ± 12.4-fold increase in B^{0}AT1 expression, consistent with its role as a trafficking facilitator of the transporter. All auxiliary proteins co-injected with B^{0}AT1 were shown to be expressed at the plasma membrane (Figure 4D). Taken together, these results suggest that, although APN increases the surface expression of B^{0}AT1, this function may be subsidiary to its role in increasing B^{0}AT1 substrate affinity, and that other auxiliary proteins, ACE2 and collectrin, play a more significant role in trafficking of the transporter.

The 2-fold increase in apparent substrate affinity and the ~2.5-fold increased surface expression of B^{0}AT1 can account for the ~4-fold increase in neutral amino acid transport initially observed at a leucine concentration of 100 μM. This conclusion was confirmed quantitatively, by inserting the corresponding data into the Michaelis–Menten equation (Table 3).

An increase in apparent substrate affinity can also manifest as an altered substrate specificity, if that increase in substrate affinity is preferential for certain substrates and not others. Co-expression of APN with B^{0}AT1 significantly increased amino-acid-induced currents for asparagine, serine and phenylalanine, which are normally lower-affinity substrates of the transporter ($P < 0.05$) (Figure 4E). All measurements were conducted at V_{max}-inducing substrate concentrations, indicating that APN either increased the capacity of the transporter for these particular substrates relative to other substrates; or, more likely, that the increase in substrate affinity is greater for these three amino acids relative to others.

Mechanism of increased substrate affinity in B^{0}AT1

Having established a close physical and functional interaction between B^{0}AT1 and APN, we hypothesized that APN may act as a molecular funnel, channelling hydrolysed *N*-terminal amino acids into the extracellular binding site of the transporter. In this case, leucine hydrolysed from the peptide substrates of APN may experience reduced competition by free leucine. To investigate this, we incubated oocytes co-expressing B^{0}AT1 and APN simultaneously with free leucine and peptide substrates Leu-Ser-Lys-Leu or trileucine. In the absence of ACE2 or collectrin (i.e. small amounts of transporter in the membrane), the combined addition of substrates increased transporter currents to a degree which, within the error of the measurements, was equivalent to the addition of currents from individually added substrates, suggesting that channelling of substrate by APN does not occur (Figure 5A). Oocytes expressing B^{0}AT1 alone exhibited no

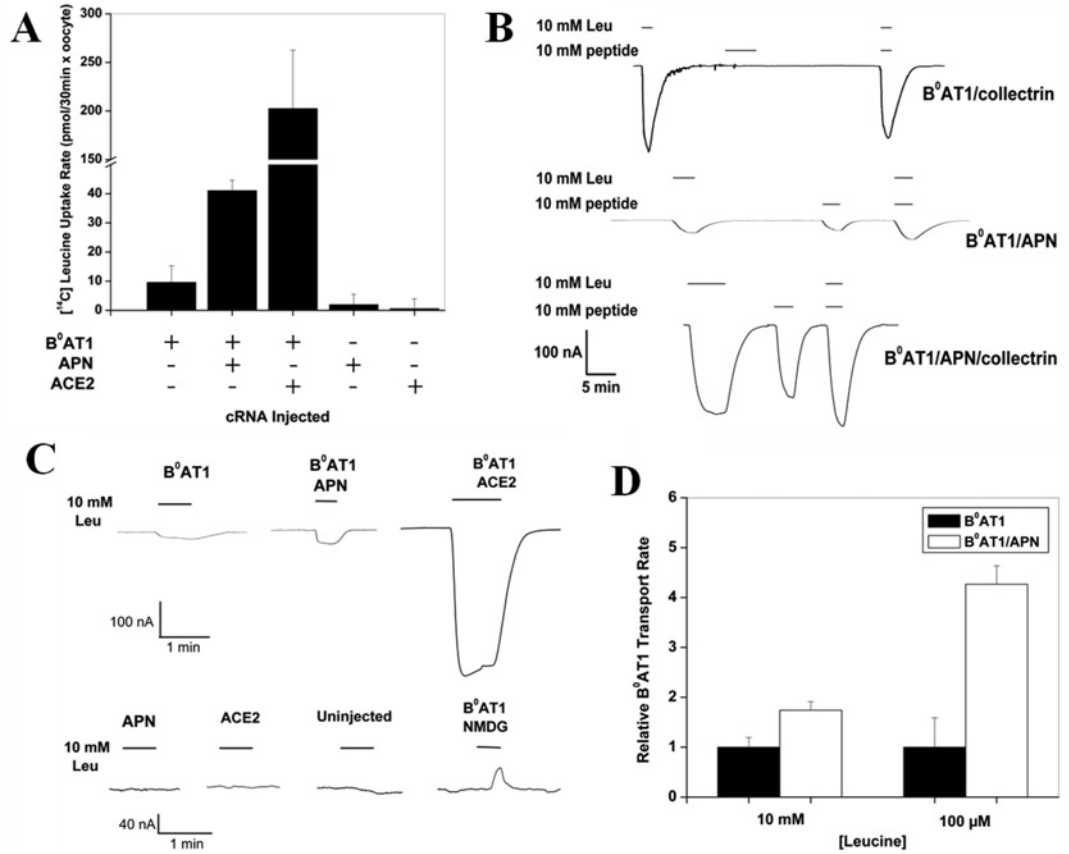

Figure 3 Effect of APN on B^0AT1 transport activity

Oocytes were injected with 10 ng of B^0AT1 cRNA, 15 ng of APN cRNA or 10 ng of ACE2 cRNA. (**A**) Uptake of 100 μM [^{14}C]leucine was measured over 30 min on day 5 post-injection. Oocyte endogenous [^{14}C]leucine uptake has been subtracted from all conditions. Each bar represents the means $\pm$ S.D. ($n = 8$–10, $e = 3$). Note that there is a break in the ordinate axis between 50 and 150 pmol/30 min per oocyte. (**B**) Oocytes were voltage-clamped at -50 mV and subsequently superfused with 10 mM leucine or Leu-Ser-Lys-Leu tetrapeptide. Substrate-induced Na^+ currents were recorded on day 5 post-injection for all oocytes, except for those co-injected with B^0AT1 and collectrin, which were recorded on day 3 or 4 post-injection. Each tracing is a typical example of currents observed in all oocytes injected with the cRNA indicated. (**C**) Oocyte substrate-induced Na^+ currents were recorded as described in (**B**) and superfused with 10 mM leucine. (**D**) Concurrent uptake and electrophysiological experiments were conducted under the same conditions as in (**A**) and (**B**), with uptake experiments using 100 μM [^{14}C]leucine and electrophysiology 10 mM unlabelled leucine. Uptake and currents under control conditions was set to 1. Each data point represents the mean $\pm$ S.D. ($n = 6$–10, $e = 3$).

response to peptide incubation, nor was there any addition of currents when both potential sources of leucine were added simultaneously. The result was different when large amounts of transporter were in the membrane due to co-expression of collectrin (Figure 5B). In contrast with Figure 5(A), the combined incubation of leucine and peptide resulted in currents that were smaller than the addition of currents from individually added substrates (Figure 5B). This result was confirmed by changing both the leucine and peptide concentration (Supplementary Figure S4 at http://www.BiochemJ.org/bj/446/bj4460135add.htm). An increase in the peptide concentration from 1 mM to 2 mM also appeared to slightly inhibit free leucine transport when both substrates were incubated together.

Since APN did not channel substrates into the transporter, we next hypothesized that the increase in apparent substrate affinity could be caused by an increase of the local substrate concentration as compared with the bulk concentration. An amino acid binding site has been observed in APN and many high-resolution structures of the *E. coli* APN have bound amino acids [40–42]. Theoretically, rapid APN-mediated binding of neutral amino acids could lead to such a local concentration increase. Incubating B^0AT1 and APN co-expressing oocytes with the peptidase inhibitor bestatin, which competes with substrate for APN's binding site, blunted the APN-mediated increase of

Table 2 Kinetic properties of B^0AT1/APN co-expressing oocytes

X. laevis oocytes where injected with the transporter and auxiliary protein indicated. The Na^+-induced currents were recorded as outlined in Figure 4. Each fitted data point represents the mean $\pm$ S.D. ($n = 6$–8, $e = 3$).

Transporter	Substrate	Auxiliary protein	I_{max} (nA $\pm$ S.D.)	Apparent K_m (mM $\pm$ S.D.)
B^0AT1	Leucine	Collectrin	523 $\pm$ 57	1.35 $\pm$ 0.17
	APN		17.4 $\pm$ 1.5	0.63 $\pm$ 0.07
B^0AT1	Glutamine	Collectrin	720 $\pm$ 111	2.56 $\pm$ 0.54
	APN		27 $\pm$ 5.6	1.17 $\pm$ 0.18
B^0AT1	Phenylalanine	Collectrin	577 $\pm$ 69	8.66 $\pm$ 1.83
	APN		22 $\pm$ 4	4.00 $\pm$ 0.43

B^0AT1-mediated leucine transport (Figure 6) ($P < 0.001$). The APN-facilitated increase in B^0AT1 activity was not entirely subdued, however, consistent with APN's role in increasing B^0AT1 surface expression.

We mutated further critical residues in the amino-acid-binding site of APN as an additional way of testing whether binding of amino acids to APN was the cause of an increase in B^0AT1 apparent substrate affinity. In order to identify the critical amino

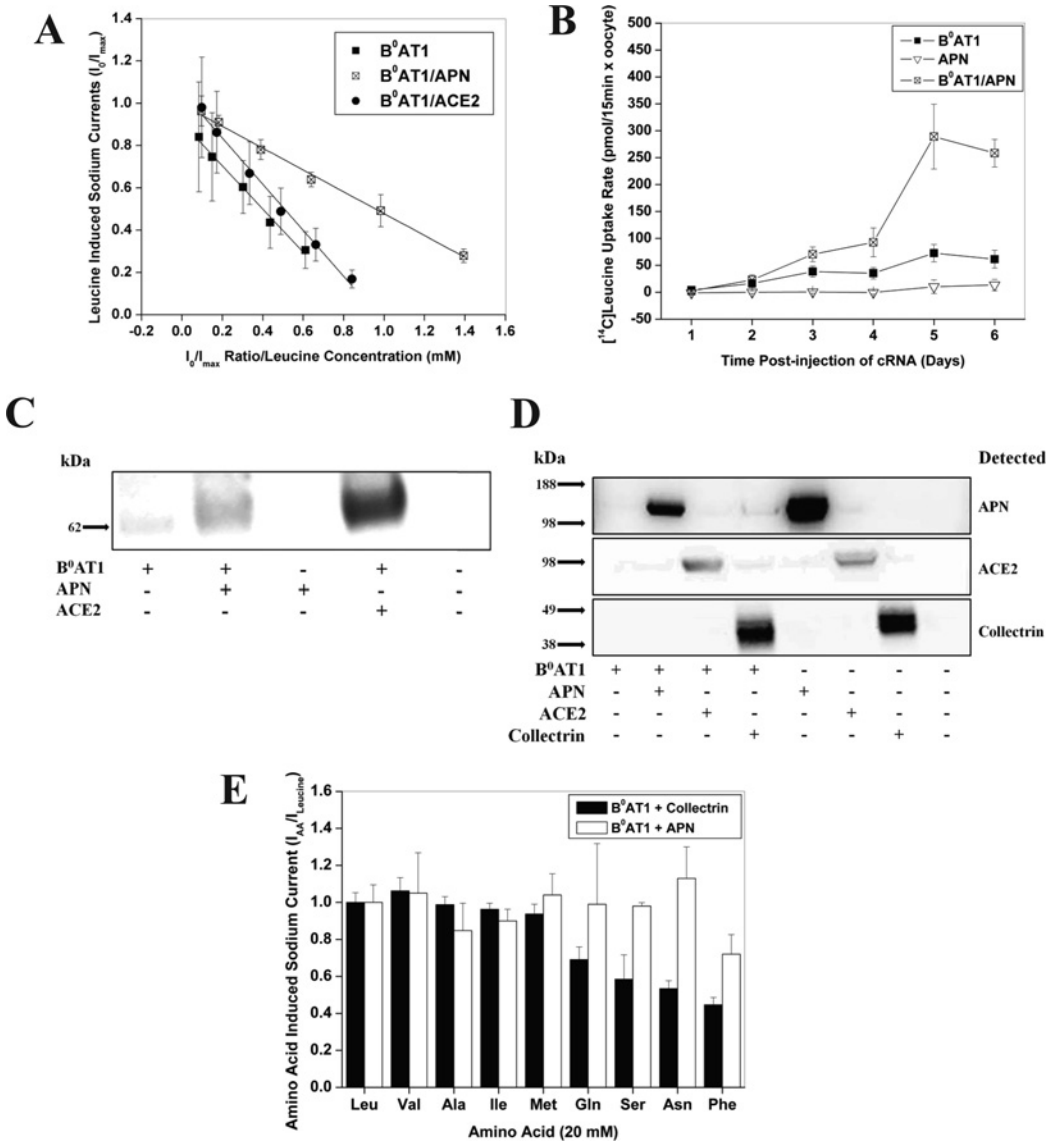

Figure 4 Changes in B^{0}AT1 transporter kinetics by APN and ACE2

Oocytes were injected with combinations of the following amounts of cRNA: B^{0}AT1, 10 ng; APN, 15 ng; ACE2, 10 ng; and collectrin, 2 ng. Leucine-induced Na^+ currents were recorded on day 5 post-injection, except those co-injected with B^{0}AT1 and ACE2, which were recorded on day 3 or 4 post-injection. (**A**) Oocytes were voltage-clamped at -50 mV and subsequently superfused with serial concentrations of leucine (0.1–10 mM) in descending and then ascending order. B^{0}AT1-expressing oocytes were not superfused with 0.1 mM leucine due to a low signal to noise ratio elicited at this concentration. An Eadie–Hofstee linear regression plot of the data points is shown. Each data point represents the mean $\pm$ S.D. ($n = 6$–8, $e = 3$). (**B**) Uptake of 100 μM [^{14}C]leucine was measured over 15 min on days 1–6 post-injection. Oocyte endogenous [^{14}C]leucine uptake has been subtracted. Each data point represents the mean $\pm$ S.D. ($n = 8$–12, $e = 3$). (**C**) A total of 15 oocytes per sample were incubated in 0.5 mg/ml sulfo-NHS-LC-biotin on day 5 post-injection before being lysed and treated with streptavadin-coated agarose beads. Samples were separated by SDS/PAGE, blotted, detected and visualized for B^{0}AT1 using immunoblot analysis. (**D**) A total of 15 oocytes per sample were prepared as in (**C**). Following SDS/PAGE, proteins were detected and visualized using immunoblot analysis for APN. Membranes were prepared for detection of subsequent proteins by stripping, re-blocking and re-probing of the protein indicated. Molecular masses are indicated to the left-hand side in kDa. (**E**) Oocytes were voltage-clamped at -50 mV and subsequently superfused with 20 mM of the amino acid (AA) indicated. All substrate-induced currents were normalized to a 20 mM leucine current (I_{Leu}) to account for transporter de-sensitization. Each bar represents the mean $\pm$ S.D. ($n = 6$–8, $e = 3$).

acid residues involved in substrate and zinc ion stabilization in murine APN, we generated a homology model based on an X-ray crystal structure of the *E. coli* LAP enzyme (PDB code 3B34) (Figures 7A and 7B). A preliminary sequence alignment of APN with potential orthologues from diverse species identified *E. coli* LAP as belonging to the aminopeptidase family of M1 class metalloproteases, with 24 % or greater sequence identity with APN (Figure 8). The aminopeptidase family is characterized by three active-site motifs: the **HE**XX**H** and B**X**L**X**E zinc-binding motifs are located 24 residues apart in all family members, and substrate binding is associated with the **G**X**MEN** motif [43]. All three motifs are fully conserved between *E. coli* LAP and APN (Figure 8). The main features of the overall structure of *E. coli* LAP were reproduced in the APN model with a backbone chain RMSD of 0.68 Å, and >95 % of dihedral angles in the allowable regions. As the N-terminus of APN is absent in *E. coli* LAP, the cytosolic N-terminus, single-pass membrane helix and linking region to the extracellular catalytic domains representing residues 1–89 are missing from the model (Figure 7B). A phenylalanine residue bound to the *E. coli* LAP crystal structure (PDB code 3B34) was superimposed into the binding site of the APN model. No steric interference was observed, suggesting that amino acid

Table 3 Validation of experimental apparent K_m values for B^0AT1 and APN co-expression

The kinetic parameters apparent K_m and I_{max} were calculated using electrophysiological recordings of the proteins indicated expressed in *X. laevis* oocytes (Figure 4A). V_{max} (mmol/min per oocyte) values were calculated from I_{max} values, and $V_{predicted}$ was calculated by substituting these values into the Michaelis–Menten function at 10 mM or 100 μM substrate concentrations ([S]). $V_{experimental}$ represents the mean ± S.E.M. from three experiments using electrophysiological and uptake experiments (Figure 3D). All rate (V) values were calculated as mmol/min per oocyte and fold-change was calculated relative to B^0AT1-expressing oocytes.

			[S] = 10 mM		[S] = 100 μM	
Protein(s) expressed in oocytes	Apparent K_m (mM ± S.D.)	I_{max} (nA ± S.D.)	$V_{predicted}$ fold-change	$V_{experimental}$ fold-change	$V_{predicted}$ fold-change	$V_{experimental}$ fold-change
B^0AT1	1.02 ± 0.06	8.09 ± 2.33	1	1	1	1
B^0AT1/APN	0.52 ± 0.02	18.78 ± 1.86	2.42	2.16 ± 0.18	4.18	4.70 ± 0.39
B^0AT1/ACE2	1.09 ± 0.04	458.90 ± 85.28	56.53	49.28 ± 5.66	53.40	45.60 ± 9.56

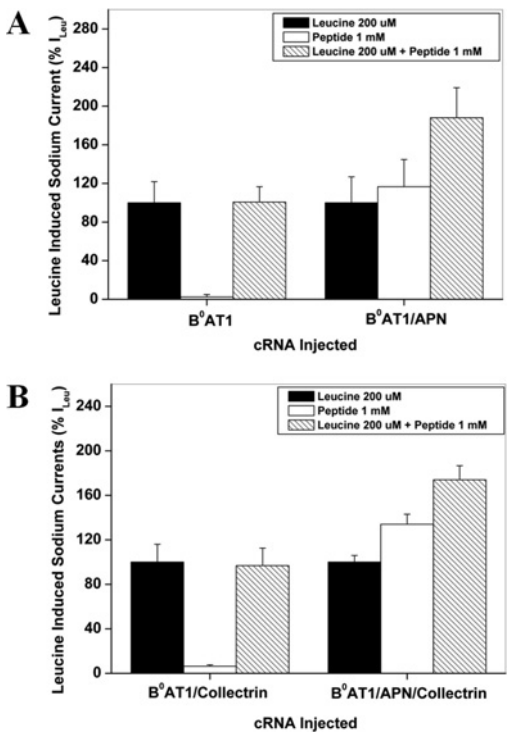

Figure 5 Mechanism of APN-mediated increase in substrate affinity of B^0AT1

Oocytes were injected with 10 ng of B^0AT1 cRNA, 15 ng of APN cRNA and 2 ng of collectrin cRNA. (**A**) Oocytes were voltage clamped at − 50 mV and subsequently superfused with either 200 μM leucine or 1 mM Leu-Ser-Lys-Leu tetrapeptide. Leucine-induced sodium currents were recorded 4–6 days post-injection. All Na^+ currents were normalized to the sodium currents elicited by 200 μM leucine (I_{Leu}) at 100 %. Each bar represents the mean ± S.D. ($n = 6$–8, $e = 3$). (**B**) Oocytes were recorded as indicated in (**A**) and superfused with either 200 μM leucine or 1 mM leucine tripeptide. All Na^+ currents were normalized to the Na^+ currents elicited by 200 μM leucine (I_{Leu}) at 100 %. Each bar represents the mean ± S.D. ($n = 18$).

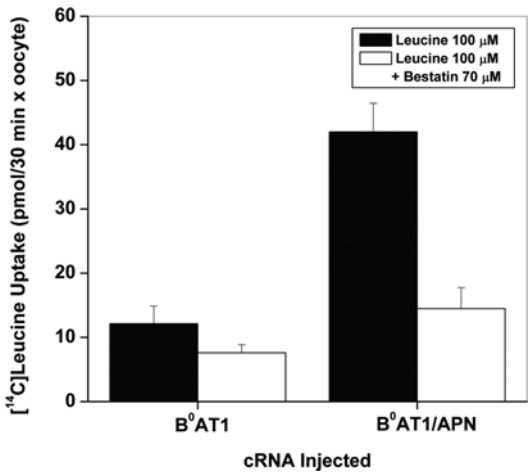

Figure 6 Mechanism of APN-mediated increase in substrate affinity of B^0AT1

Oocytes were injected with either 10 ng of B^0AT1 cRNA or 15 ng of APN cRNA. Uptake of [^{14}C]leucine was measured over 30 min on day 5 post-injection. Bestatin (70 μM) was pre-incubated for 1 min before leucine was added. Oocyte endogenous leucine transport has been subtracted in all experimental conditions. Uptake was normalized to that measured in oocytes expressing B^0AT1 alone in the presence of 100 μM leucine. Each bar represents the mean ± S.E.M. of data combined from four experiments ($n = 33$–38).

substrates are likely to bind in a similar manner in both enzymes. This hypothesis is supported by the conservation of the binding site motif.

Four single-residue APN mutants were generated and co-expressed with B^0AT1 in *X. laevis* oocytes to examine their effects on the transporter's K_m. Mutation E354A affects a highly conserved substrate-binding residue. Mutations E388A and E410A are conserved zinc-co-ordinating residues. All three mutations were designed to abolish all catalytic activity of APN. The fourth mutant, Y476F, also highly conserved, was considered to fulfil a less critical substrate-binding role and was introduced as a potential partial loss-of-function mutation. Surprisingly, all mutants exhibited various levels of catalytic activity as indicated by peptide-induced currents (Figure 9A). APN Y476F exhibited wild-type-like activity, at the other extreme APN E354A had lost approximately 80 % of its catalytic activity. A kinetic analysis of leucine uptake into oocytes co-expressing mutant APN and B^0AT1 showed an inverse correlation between the catalytic activity of the APN mutants and their ability to alter B^0AT1's apparent K_m ($r = -0.84$, $P = 0.035$, $n = 74$) (Figure 9B). The mutant with the least catalytic activity, E354A, also displayed the least alteration in apparent substrate affinity of B^0AT1-mediated transport compared with oocytes expressing B^0AT1 alone or B^0AT1 and collectrin. Conversely, the mutants E388A and Y476F, retaining most of the wild-type's catalytic activity, increased the apparent substrate affinity of B^0AT1 to the same extent as wild-type APN. B^0AT1 surface expression was similar across all oocytes co-expressing wild-type APN or the mutants, suggesting that APN's role as a trafficking facilitator is unaffected in all mutants tested (Figure 9C).

DISCUSSION

We have demonstrated that the major neutral amino acid transporter of the mammalian small intestine and kidney

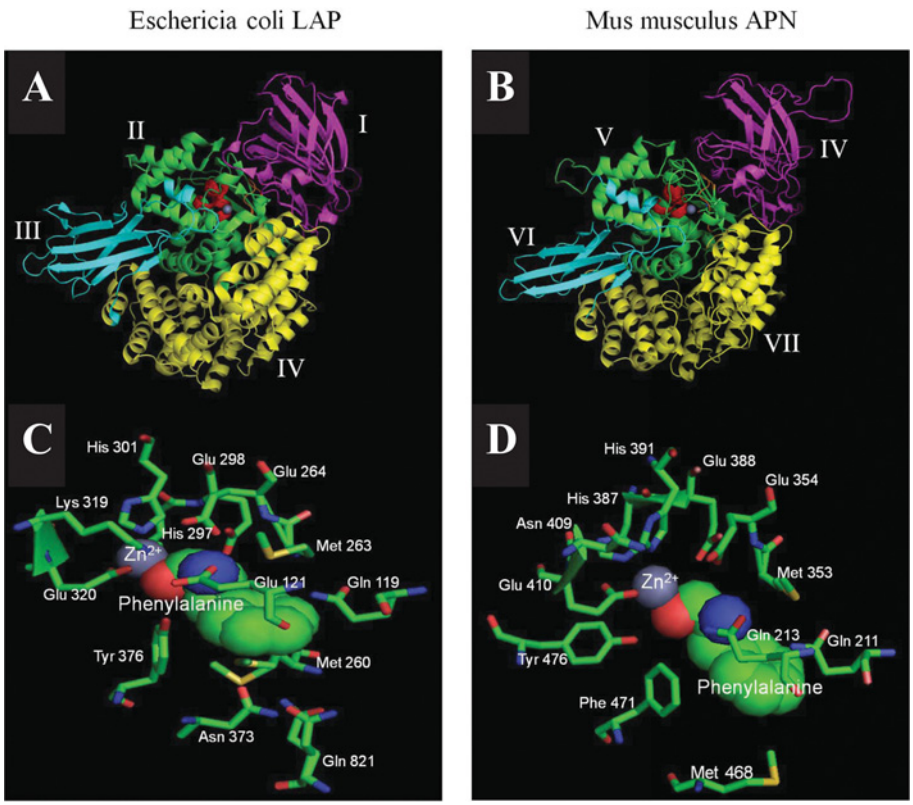

Figure 7 Homology model of mouse APN

The homology model of mouse APN was generated using HHpred Homology detection and structure prediction tool (Max-Planck Institute for Developmental Biology; http://toolkit.tuebingen.mpg.de/hhpred) and visualized using PyMOL v9.9 (DeLano Scientific; http://www.pymol.org). Depicted are *E. coli* LAP (PDB code 3B34) (**A**) and murine APN (**B**) with phenylalanine bound to their active site. The top panels display a lateral three-dimensional view of the murine and *E. coli* structures. Domains are shaded as follows: magenta (domain I for *E. coli*, domain IV for mouse); green (domain II for *E. coli*, domain V for mouse); cyan (domain III for *E. coli*, domain VI for mouse); and yellow (domain IV for *E. coli*, domain VII for mouse). Domains I–III from mouse APN are not depicted (residues 1 to 89) as no homologous sequence exists in *E. coli* for these. The HEXXH . . . . . .BXLXE and GXMEN consensus sequences for zinc and amino acid binding are shaded red and orange respectively. The zinc ion is shaded blue-grey. The active sites of *E. coli* LAP and murine APN are depicted in panels (**C**) and (**D**) respectively. The zinc ion is shaded blue-grey, and the bound phenylalanine is depicted as a space-filled model, with oxygen and nitrogen atoms coloured red and blue respectively. All residues predicted to bind and interact with the substrate are shown and labelled.

Species and Enzyme/Receptor				Accession Number
Mus musculus APN	349	NAGAMENWGLVTYRESSLVFDSQSSSISNKERVVTVIAHELAHQWFGNLVTVAWWNDLWLNEGFASYVEYLGADYA--EP	426	P97449
E.coli LAP	259	NMGAMENKGLNIFNSKYVLARTDTATDKDYLDIERVIGHEYFHNWTGNRVTCRDWFQLSLKEGLTVFRDQEFSSDLGSRA	338	P04825
Human APN	350	NAGAMENWGLVTYRENSLLFDPLSSSSSNKERVVTVIAHELAHQWFGNLVTIEWWNDLWLNEGFASYVEYLGADYA--EP	427	P15144
S.cerevisiae AP	358	SAGAMENWGLVTYRVVDLLLDKDNSTLDRIQRVAEVVQHELAHQWFGNLVTMDWWEGLWLNEGFATWMSWYSCNEF--QP	435	P32454
L.lactis AP	250	SAGAMENWGCITYREVCMLVDPENATIQSKQYVATVIAHELAHQWFGDLVTMQWWDDLWLNESFANNMEYVCMDAL--EP	327	A2RI32
L.delbruckii lysyl AP	250	SAGAMENWGLVTYREAYLLLDPDNTTLEMKKLVATVVTHELAHQWFGDLVTMEWWDNLWLNESFANMMEYLSVDHL--EP	327	P37896
R.norvegicus (Rat) APN	349	NAGAMENWGLVTYRESALVFDPQSSSISNKERVVTVIAHELAHQWFGNLVTVDWWNDLWLNEGFASYVEFLGADYA--EP	426	P15684
Sus Scrofa (Porcine) APN	345	NAGAMENWGLVTYRENALLFDPQSSSISNKERVVTVIAHELAHQWFGNLVTLAWWNDLWLNEGFASYVEYLGADHA--EP	422	P15145
Felis catus (Cat) APN	349	NAGAMENWGLVTYRESALLYDRQSSSSGNQERVVTVIAHELAHQWFGNLVTLEWWNDLWLNEGFASYVEYLGADFA--EP	426	P79171
O.cuniculus (Rabbit) APN	346	NAGAMENWGLVTYRESALLFDPLVSSISNKERVVTVVAHELAHQWFGNLVTVDWWNDLWLNEGFASYVEYLGADYA--EP	423	P15541
Bos Taurus (Bovine) APN	347	NAGAMENWGLVTYRENALLYDPQSSSSSNKERVVTVIAHELAHQWFGNLVTLAWWNDLWLNEGFASYVEYLGADYA--EP	424	P79098
Mus Musculus APA	347	GTGAMENWGLVTYRETNLLYDPLLSASSNQQRVASVVAHELVHQWFGNTVTMDWWDDLWLNEGFASFFEFLGVNHA--EK	424	Q52JJ6
Human LTA4	267	PYGGMENP-CLTFVTPTLLAGDKSLSN--------VIAHEISHSWTGNLVTNKTWDHFWLNEGHTVYLERHICGRLFGEK	337	P09960
S.cerevisiae AAP1	262	SAGAMENWGLVTYRVIDLLLDIENSSLDRIQRVAEVIQHELAHQWFGNLVTMDWWEGLWLNEGFATWMSWYSCNKF--QP	339	P37898
Consensus Sequence		GXMEN VBXHEBXHXWXGXXVTXXXWXXBXLXE		

substrate-binding domain

zinc-binding domains

Figure 8 Sequence alignments of aminopeptidase family members

Potential homologues of mouse APN (P97449) were identified by a NCBI blastp search. Peptide sequences were aligned using COBALT (http://www.ncbi.nlm.nih.gov/tools/cobalt/cobalt.cgi?CMD=Web). Highly conserved regions are boxed. In the consensus sequence row, X is any amino acid and B is bulky side chain neutral amino acids. The full-length aligned sequence from *E. coli* LAP (not shown) was used as the basis for the homology modelling of mouse APN. The three conserved residues in the binding domains of murine APN selected for site-directed mutagenesis are indicated with a vertical line above them, a fourth mutated residue, Tyr^{476}, is not shown. AAP1, alanine/arginine aminopeptidase 1; LTA4, leukotriene A-4 hydrolase.

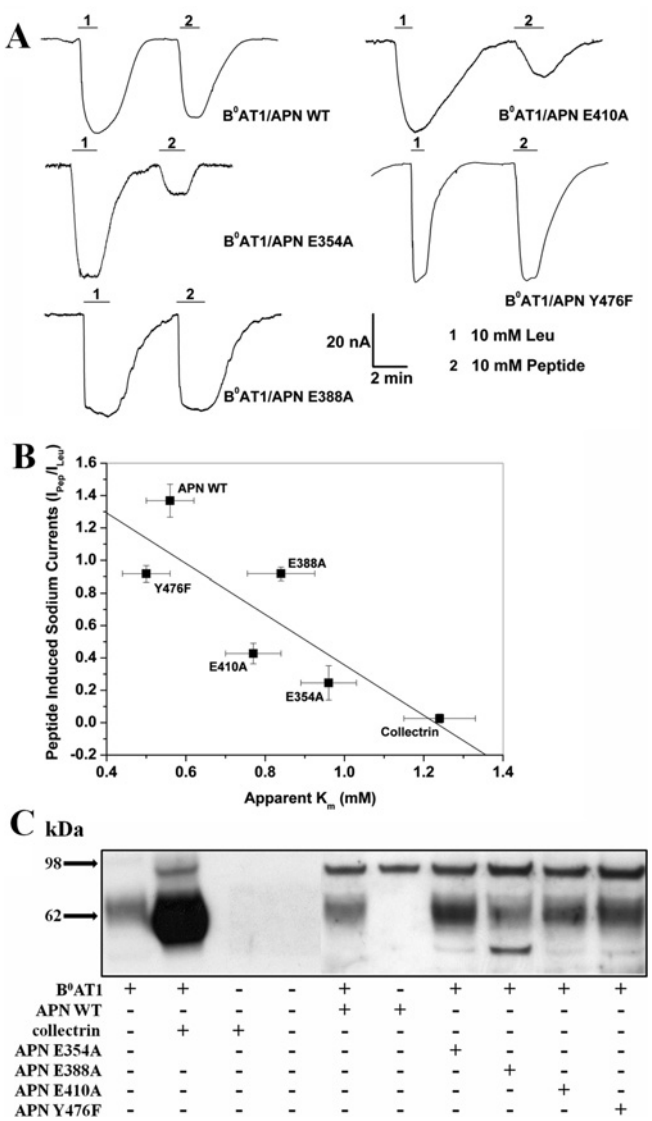

Figure 9 Mechanism of APN-mediated increase in substrate affinity of B^0AT1

Oocytes were injected with either 10 ng of B^0AT1 cRNA, 15 ng of APN cRNA or 2 ng of collectrin cRNA. (**A**) Oocytes were voltage clamped at -50 mV and subsequently superfused with either 10 mM leucine or 10 mM Leu-Ser-Lys-Leu tetrapeptide. Each tracing is a typical example of currents observed in all oocytes injected with the cRNA indicated. Leucine-induced sodium currents were recorded on day 4 and 5 post-injection for all oocytes. (**B**) Oocytes were recorded as indicated in (**A**). Each data point indicates an APN mutant co-expressed with B^0AT1, or B^0AT1 co-expressed with collectrin. All peptide-induced sodium currents were normalized to the corresponding leucine-induced Na^+ current (I_{Pep}/I_{Leu}). Each data point represents the mean $\pm$ S.D. for both peptide-induced sodium currents and apparent K_m values. The trend line was fitted using linear regression ($r = -0.84$, $P = 0.035$ and $n = 74$). (**C**) A total of 15 oocytes/sample were incubated in 0.5 mg/ml sulfo-NHS-LC-biotin on day 5 post-injection before being lysed and treated with streptavadin-coated agarose beads. Samples were separated by SDS/PAGE. Subsequently B^0AT1 was detected by immunoblotting. Molecular masses are indicated to the left-hand side in kDa.

brush-border, B^0AT1, forms protein complexes with the brush-border peptidases APN and ACE2. Co-expression of these peptidases affected the kinetic parameters of B^0AT1-mediated transport differentially. APN increases the surface expression (V_{max}) to a small extent and increases the apparent substrate affinity (lower apparent K_m) of B^0AT1 transport activity. ACE2 is the primary trafficking subunit of B^0AT1 in the intestine, but did not modify the apparent substrate affinity, confirming previous results by us and others [10,11], suggesting that the formation of functional protein complexes between neutral amino acid transporters and peptidases may be a widespread phenomenon. Our results suggest that these complexes are likely to increase the efficiency of protein absorption by increasing the local substrate concentration for B^0AT1.

The extent to which membrane complexes can be investigated is limited by the membrane solubilization step, which will also interfere with protein–protein interactions. This is exemplified by the different complexes observed when using two different detergents, digitonin and Triton-X100. Thus the complex between B^0AT1, APN and ACE2 should be viewed as a core complex of yet unknown stoichiometry. In agreement with this notion, different APN-associated complexes have been isolated previously [19,20,44,45]. Using 10 % dodecylmaltoside at 4 °C, Babusiak et al. [19] isolated several APN-containing complexes, which included maltase–glucoamylase, sucrose–isomaltase, endopeptidase-2 and, surprisingly, subunits of the Na^+/K^+-ATPase. B^0AT1 was found to be complexed with villin, microsomal triglyceride transfer protein, α-actinin-4 and protein disulphide isomerise, but not with APN. This may be due to the different solubilization conditions used, or because mice were starved for 24 h before being euthanized, a condition previously shown to have multiple effects on the composition and structural integrity of the intestinal brush-border [46]. Likewise, isolation of proteins from lipid rafts has been performed using a diversity of experimental conditions and tissue sources [47]. Originally, as we have performed in the present study, BBMV rafts from the intestinal brush-border were isolated using Triton X-100 at 0–4 °C [29,48]. In addition, rafts have been isolated using Triton X-100 at different temperatures [49], or with different detergents from both primary tissue and cultured epithelial cell lines [50–52]. Furthermore, evidence exists for different types of rafts or micro-domains containing cholesterol, but others are composed of less cholesterol and high quantities of glycolipids stabilized by galectin-4, which binds the extracellular carbohydrate motifs of heavily glycosylated membrane peptidases [20,47,52]. As APN is heavily glycosylated [14,53] and is a major component of the glycolipid-rich rafts [20,29,44], it is tempting to speculate that the complexes identified in the present study are stabilized and trafficked by a galectin-4-dependent mechanism. B^0AT1 has also been shown to contain N-glycosylation sites in its extracellular loops [54]. To our knowledge, no study isolating apical complexes have yet identified B^0AT1, APN or ACE2 as co-components of a brush-border complex, either in the apical membrane or as part of a stable trafficking unit. The combination of these three proteins is restricted to the intestine. There is limited overlap of ACE2 and B^0AT1 expression in the kidney, where the transporter is mainly associated with collectrin [55]. Recently, alterations in substrate affinity for alanine, a major B^0AT1 substrate, were also demonstrated over widespread sections of rat small intestine incubated in more proximal sections with the same amino acids that displayed affinity alterations [56].

Overall, we establish a possible mechanism by which APN alters the apparent substrate affinity of B^0AT1, namely, by increasing the local concentration of neutral amino acids at the plasma membrane, thereby causing an 'apparent' change in the transporter's K_m. Such a mechanism is not uncommon in nature, and is reminiscent of numerous periplasmic binding proteins and ABC (ATP-binding cassette) primary transporters in archeal and bacterial species [57–61]. This local concentration variation and change in 'apparent' K_m is also observed in the 'proton well' effect of some proton-translocating ATPases [62]. Homology modelling and structural data of *E. coli* LAP [40,42] suggest that APN possesses a binding site for neutral amino

acids. Several large neutral amino acids have been crystallized in the *E. coli* LAP-binding pocket, demonstrating that the active site of LAP lies in a groove that runs between the two lobes of domain II, and is covered by domain IV [40–42]. From sequence identity, structural homology and biochemical analysis, we demonstrate that the APN active site is homologous with LAP. This basic geometry of the *E. coli* active site and narrowness of the substrate entry site are both conserved in mouse APN and mutagenesis of the substrate binding site abolishes the effect on transporter affinity. The increase of the local concentration is expected to become more relevant as the peptidase to transporter ratio increases. This was confirmed by the oocyte experiments, where peptidase-induced currents were additive to the currents induced by bulk leucine at low surface concentrations of B^0AT1 (Figure 6A). When the B^0AT1 concentration was increased relative to a constant amount of APN, the currents were no longer additive. This model does not rule out the possibility that APN increases the transporter's substrate affinity by altering the thermodynamics of substrate binding, whether through direct (B^0AT1 binding site) or allosteric means.

In the present study we have demonstrated the presence of digestive protein complexes in the intestinal brush-border containing the peptidases APN and ACE2 and the neutral amino acid transporter B^0AT1. On the basis of our results, we propose these complexes to function as a metabolon, which optimises protein digestive and absorption processes at the brush-border. We envision a scenario where B^0AT1 trafficking and expression in the membrane is largely dependent on ACE2, whereas optimal, or adaptive, functioning to changing dietary conditions requires association with APN. It appears likely that these complexes contain a wider array of proteins than shown in the present study, and the full elucidation of their components, functional significance, and prevalence in main absorptive epithelial surfaces of the body are subjects for further study.

AUTHOR CONTRIBUTION

Stephen Fairweather performed and designed the experiments and wrote the paper. Angelika Bröer performed the experiments. Megan O'Mara refined and validated the APN homology model. Stephan Bröer designed and co-ordinated the study and experiments, and edited the paper prior to submission.

ACKNOWLEDGEMENTS

We thank the laboratory of Dr Michael Ryan (La Trobe University), especially Crista George, Matthew McKenzie, and Nora Vögtle for their assistance with Blue native electrophoresis. We also thank Stephen Michnick (Université de Montréal) for providing the original Venus fly trap vectors. We are indebted to Cathy Gillespie (Australian National University) for assistance with confocal microscopy, and to Salik Ali and Teresa Neeman for support with statistical analysis. We also thank Sarojini Balkrishna, Torsten Juelich, Farid Rahimi and Emrah Tumer for paper editing prior to submission, and Ariel Moisis, Hector Rodriguez and Uschi Wiedemann for general assistance and technical support.

FUNDING

This study was supported by the National Health and Medical Research Council [grant number 525415].

REFERENCES

1 Boron, W. F. and Boulpeap, E. L. (2003) Medical Physiology, p. 934, Saunders, Philadelphia
2 Tyska, M. J., Mackey, A. T., Huang, J. D., Copeland, N. G., Jenkins, N. A. and Mooseker, M. S. (2005) Myosin-1a is critical for normal brush border structure and composition. Mol. Biol. Cell **16**, 2443–2457
3 Mentlein, R. (2004) Cell-surface peptidases. Int. Rev. Cytol. **235**, 165–213
4 Alpers, D. H. (1987) Digestion and absorption of carbohydrates and proteins. In Physiology of The Gastro-intestinal Tract (Johnson, L. R., ed.), pp. 1469–1487, Raven Press, New York
5 Broer, S. (2009) The role of the neutral amino acid transporter B0AT1 (SLC6A19) in Hartnup disorder and protein nutrition. IUBMB Life **61**, 591–599
6 Broer, S. (2008) Amino acid transport across mammalian intestinal and renal epithelia. Physiol. Rev. **88**, 249–286
7 Seow, H. F., Broer, S., Broer, A., Bailey, C. G., Potter, S. J., Cavanaugh, J. A. and Rasko, J. E. (2004) Hartnup disorder is caused by mutations in the gene encoding the neutral amino acid transporter SLC6A19. Nat. Genet. **36**, 1003–1007
8 Scriver, C. R. (1965) Hartnup Disease: a genetic modification of intestinal and renal transport of certain neutral alpha-amino acids. N. Engl. J. Med. **273**, 530–532
9 Matthews, D. M. (1991) Protein Absorption. Wiley-Liss, New York
10 Camargo, S. M., Singer, D., Makrides, V., Huggel, K., Pos, K. M., Wagner, C. A., Kuba, K., Danilczyk, U., Skovby, F., Kleta, R. et al. (2009) Tissue-specific amino acid transporter partners ACE2 and collectrin differentially interact with hartnup mutations. Gastroenterology **136**, 872–882
11 Kowalczuk, S., Broer, A., Tietze, N., Vanslambrouck, J. M., Rasko, J. E. and Broer, S. (2008) A protein complex in the brush-border membrane explains a Hartnup disorder allele. FASEB J. **22**, 2880–2887
12 Singer, D., Camargo, S. M., Huggel, K., Romeo, E., Danilczyk, U., Kuba, K., Chesnov, S., Caron, M. G., Penninger, J. M. and Verrey, F. (2009) Orphan transporter SLC6A18 is renal neutral amino acid transporter B0AT3. J. Biol. Chem. **284**, 19953–19960
13 Plakidou-Dymock, S., Tanner, M. J. and McGivan, J. D. (1993) A role for aminopeptidase N in Na^+-dependent amino acid transport in bovine renal brush-border membranes. Biochem. J. **290**, 59–65
14 Riemann, D., Kehlen, A. and Langner, J. (1999) CD13–not just a marker in leukemia typing. Immunol. Today **20**, 83–88
15 Sjostrom, H., Noren, O. and Olsen, J. (2000) Structure and function of aminopeptidase N. Adv. Exp. Med. Biol. **477**, 25–34
16 Olsen, J., Kokholm, K., Noren, O. and Sjostrom, H. (1997) Structure and expression of aminopeptidase N. Adv. Exp. Med. Biol. **421**, 47–57
17 Bohmer, C., Broer, A., Munzinger, M., Kowalczuk, S., Rasko, J. E., Lang, F. and Broer, S. (2005) Characterization of mouse amino acid transporter B0AT1 (slc6a19). Biochem. J. **389**, 745–751
18 Mina-Osorio, P. (2008) The moonlighting enzyme CD13: old and new functions to target. Trends Mol. Med. **14**, 361–371
19 Babusiak, M., Man, P., Petrak, J. and Vyoral, D. (2007) Native proteomic analysis of protein complexes in murine intestinal brush border membranes. Proteomics **7**, 121–129
20 Danielsen, E. M. and van Deurs, B. (1997) Galectin-4 and small intestinal brush border enzymes form clusters. Mol. Biol. Cell **8**, 2241–2251
21 Alfalah, M., Jacob, R. and Naim, H. Y. (2002) Intestinal dipeptidyl peptidase IV is efficiently sorted to the apical membrane through the concerted action of *N*- and *O*-glycans as well as association with lipid microdomains. J. Biol. Chem. **277**, 10683–10690
22 Alfalah, M., Jacob, R., Preuss, U., Zimmer, K. P., Naim, H. and Naim, H. Y. (1999) *O*-linked glycans mediate apical sorting of human intestinal sucrase-isomaltase through association with lipid rafts. Curr. Biol. **9**, 593–596
23 Spodsberg, N., Alfalah, M. and Naim, H. Y. (2001) Characteristics and structural requirements of apical sorting of the rat growth hormone through the O-glycosylated stalk region of intestinal sucrase-isomaltase. J. Biol. Chem. **276**, 46597–46604
24 Li, X., Galli, T., Leu, S., Wade, J. B., Weinman, E. J., Leung, G., Cheong, A., Louvard, D. and Donowitz, M. (2001) Na^+-H^+ exchanger 3 (NHE3) is present in lipid rafts in the rabbit ileal brush border: a role for rafts in trafficking and rapid stimulation of NHE3. J. Physiol. **537**, 537–552
25 Biber, J., Stieger, B., Stange, G. and Murer, H. (2007) Isolation of renal proximal tubular brush-border membranes. Nat. Protoc. **2**, 1356–1359
26 Redondo, F. L., Pascual, T., Bergon, E. and Miravalles, E. (1986) L-alanine-4-nitroanilide as a substrate for microsomal aminopeptidase. Clin. Chem. **32**, 912–913
27 Lottenberg, R. and Jackson, C. M. (1983) Solution composition dependent variation in extinction coefficients for p-nitroaniline. Biochim. Biophys. Acta **742**, 558–564
28 Schagger, H. and von Jagow, G. (1991) Blue native electrophoresis for isolation of membrane protein complexes in enzymatically active form. Anal. Biochem. **199**, 223–231
29 Danielsen, E. M. (1995) Involvement of detergent-insoluble complexes in the intracellular transport of intestinal brush border enzymes. Biochemistry **34**, 1596–1605
30 Danielsen, E. M. and van Deurs, B. (1995) A transferrin-like GPI-linked iron-binding protein in detergent-insoluble noncaveolar microdomains at the apical surface of fetal intestinal epithelial cells. J. Cell Biol. **131**, 939–950
31 Waugh, M. G. and Hsuan, J. J. (2009) Preparation of membrane rafts. In Lipid Signaling Protocols (Larijani, B., ed.), pp. 403–414, Humana Press, Totowa

32 Broer, S. (2003) *Xenopus laevis* oocytes. In Membrane Transporters: Methods and Protocols (Yan, Q., ed.), pp. 245–258, Humana Press, Totowa
33 Rich, D. H., Moon, B. J. and Harbeson, S. (1984) Inhibition of aminopeptidases by amastatin and bestatin derivatives. Effect of inhibitor structure on slow-binding processes. J. Med. Chem. **27**, 417–422
34 Ghosh, I., Hamilton, A. D. and Regan, L. (2000) Antiparallel leucine zipper-directed protein reassembly: application to the green fluorescent protein. J. Am. Chem. Soc. **122**, 2
35 O'Mara, M. L. and Tieleman, D. P. (2007) P-glycoprotein models of the apo and ATP-bound states based on homology with Sav1866 and MalK. FEBS Lett. **581**, 4217–4222
36 Vriend, G. (1990) WHAT IF: a molecular modeling and drug design program. J. Mol. Graphics **8**, 52–56
37 Laskowski, R. A., MacArthur, M. W., Moss, D. S. and Thornton, J. M. (1993) PROCHECK: a program to check the stereochemical quality of protein structures. J. Appl. Crystallogr. **26**, 9
38 Broer, A., Klingel, K., Kowalczuk, S., Rasko, J. E., Cavanaugh, J. and Broer, S. (2004) Molecular cloning of mouse amino acid transport system B0, a neutral amino acid transporter related to Hartnup disorder. J. Biol. Chem. **279**, 24467–24476
39 Camargo, S. M., Makrides, V., Virkki, L. V., Forster, I. C. and Verrey, F. (2005) Steady-state kinetic characterization of the mouse B^0AT1 sodium-dependent neutral amino acid transporter. Pflugers Arch. **451**, 338–348
40 Addlagatta, A., Gay, L. and Matthews, B. W. (2008) Structural basis for the unusual specificity of *Escherichia coli* aminopeptidase N. Biochemistry **47**, 5303–5311
41 Addlagatta, A., Gay, L. and Matthews, B. W. (2006) Structure of aminopeptidase N from *Escherichia coli* suggests a compartmentalized, gated active site. Proc. Natl. Acad. Sci. U.S.A. **103**, 13339–13344
42 Ito, K., Nakajima, Y., Onohara, Y., Takeo, M., Nakashima, K., Matsubara, F., Ito, T. and Yoshimoto, T. (2006) Crystal structure of aminopeptidase N (proteobacteria alanyl aminopeptidase) from *Escherichia coli* and conformational change of methionine 260 involved in substrate recognition. J. Biol. Chem. **281**, 33664–33676
43 Hooper, N. M. (1994) Families of zinc metalloproteases. FEBS Lett. **354**, 1–6
44 Nguyen, H. T., Amine, A. B., Lafitte, D., Waheed, A. A., Nicoletti, C., Villard, C., Letisse, M., Deyris, V., Roziere, M., Tchiakpe, L. et al. (2006) Proteomic characterization of lipid rafts markers from the rat intestinal brush border. Biochem. Biophys. Res. Commun. **342**, 236–244
45 Stechly, L., Morelle, W., Dessein, A. F., Andre, S., Grard, G., Trinel, D., Dejonghe, M. J., Leteurtre, E., Drobecq, H., Trugnan, G. et al. (2009) Galectin-4-regulated delivery of glycoproteins to the brush border membrane of enterocyte-like cells. Traffic **10**, 438–450
46 Ihara, T., Tsujikawa, T., Fujiyama, Y., Ueyama, H., Ohkubo, I. and Bamba, T. (2000) Enhancement of brush border membrane peptidase activity in rat jejunum induced by starvation. Pflugers Arch. **440**, 75–83
47 Danielsen, E. M. and Hansen, G. H. (2008) Lipid raft organization and function in the small intestinal brush border. J. Physiol. Biochem. **64**, 377–382
48 Brown, D. A. and Rose, J. K. (1992) Sorting of GPI-anchored proteins to glycolipid-enriched membrane subdomains during transport to the apical cell surface. Cell **68**, 533–544
49 Braccia, A., Villani, M., Immerdal, L., Niels-Christiansen, L. L., Nystrom, B. T., Hansen, G. H. and Danielsen, E. M. (2003) Microvillar membrane microdomains exist at physiological temperature. Role of galectin-4 as lipid raft stabilizer revealed by 'superrafts'. J. Biol. Chem. **278**, 15679–15684
50 Mirre, C., Monlauzeur, L., Garcia, M., Delgrossi, M. H. and Le Bivic, A. (1996) Detergent-resistant membrane microdomains from Caco-2 cells do not contain caveolin. Am. J. Physiol. **271**, C887–C894
51 Roepstorff, K., Thomsen, P., Sandvig, K. and van Deurs, B. (2002) Sequestration of epidermal growth factor receptors in non-caveolar lipid rafts inhibits ligand binding. J. Biol. Chem. **277**, 18954–18960
52 Roper, K., Corbeil, D. and Huttner, W. B. (2000) Retention of prominin in microvilli reveals distinct cholesterol-based lipid micro-domains in the apical plasma membrane. Nat. Cell Biol. **2**, 582–592
53 O'Connell, P. J., Gerkis, V. and d'Apice, A. J. (1991) Variable O-glycosylation of CD13 (aminopeptidase N). J. Biol. Chem. **266**, 4593–4597
54 Romeo, E., Dave, M. H., Bacic, D., Ristic, Z., Camargo, S. M., Loffing, J., Wagner, C. A. and Verrey, F. (2006) Luminal kidney and intestine SLC6 amino acid transporters of B0AT-cluster and their tissue distribution in *Mus musculus*. Am. J. Physiol. Renal Physiol. **290**, F376–F383
55 Vanslambrouck, J. M., Broer, A., Thavyogarajah, T., Holst, J., Bailey, C. G., Broer, S. and Rasko, J. E. (2010) Renal imino acid and glycine transport system ontogeny and involvement in developmental iminoglycinuria. Biochem. J. **428**, 397–407
56 Mourad, F. H., Barada, K. A., Khoury, C., Hamdi, T., Saade, N. E. and Nassar, C. F. (2009) Amino acids in the rat intestinal lumen regulate their own absorption from a distant intestinal site. Am. J. Physiol. Gastrointest. Liver Physiol. **297**, G292–G298
57 Lee, S. J., Bohm, A., Krug, M. and Boos, W. (2007) The ABC of binding-protein-dependent transport in Archaea. Trends Microbiol. **15**, 389–397
58 Higgins, C. F. (2001) ABC transporters: physiology, structure and mechanism–an overview. Res. Microbiol. **152**, 205–210
59 Tame, J. R., Dodson, E. J., Murshudov, G., Higgins, C. F. and Wilkinson, A. J. (1995) The crystal structures of the oligopeptide-binding protein OppA complexed with tripeptide and tetrapeptide ligands. Structure **3**, 1395–1406
60 Nickitenko, A. V., Trakhanov, S. and Quiocho, F. A. (1995) 2 Å resolution structure of DppA, a periplasmic dipeptide transport/chemosensory receptor. Biochemistry **34**, 16585–16595
61 Tame, J. R., Murshudov, G. N., Dodson, E. J., Neil, T. K., Dodson, G. G., Higgins, C. F. and Wilkinson, A. J. (1994) The structural basis of sequence-independent peptide binding by OppA protein. Science **264**, 1578–1581
62 Maloney, P. C. (1982) Energy coupling to ATP synthesis by the proton-translocating ATPase. J. Membr. Biol. **67**, 1–12

Received 17 February 2012/23 May 2012; accepted 7 June 2012
Published as BJ Immediate Publication 7 June 2012, doi:10.1042/BJ20120307

Biochem. J. (2012) **446**, 135–148 (Printed in Great Britain) doi:10.1042/BJ20120307

online data

SUPPLEMENTARY ONLINE DATA

Intestinal peptidases form functional complexes with the neutral amino acid transporter B^0AT1

Stephen J. FAIRWEATHER*, Angelika BRÖER*, Megan L. O'MARA† and Stefan BRÖER*[1]

*Research School of Biology, Australian National University, Canberra, ACT 0200, Australia, and †School of Chemistry and Molecular Biosciences, University of Queensland, Brisbane, QLD 4072, Australia

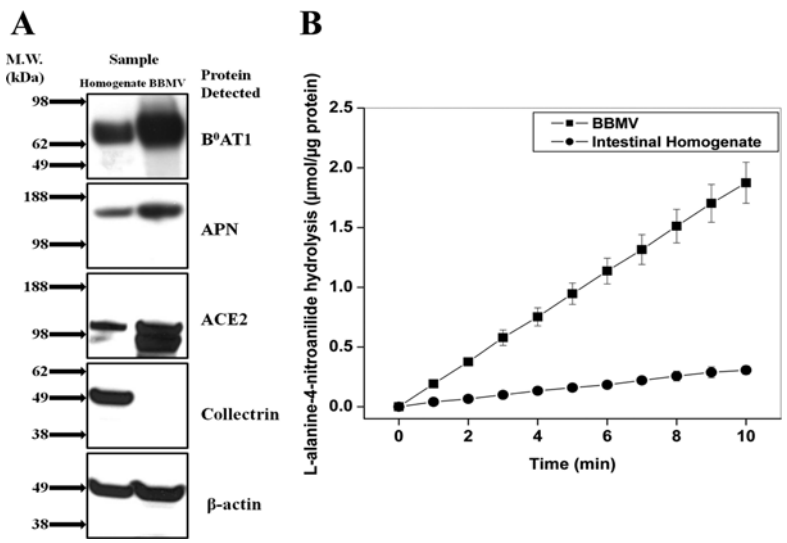

Figure S1 Isolation of intestinal brush-border protein complexes

Murine intestinal BBMVs were prepared using $MgCl_2$ precipitation and density-gradient centrifugation as described in the Experimental section of the main text. (**A**) BBMV protein (20 μg) was separated by SDS/PAGE. Following semi-dry transfer on to a nitrocellulose membrane and blocking, individual proteins were detected and visualized using immunoblot analysis. Detection was carried out following every BBMV preparation. Molecular masses are indicated to the left-hand side in kDa. (**B**) APN in BBMVs and intestinal homogenate was measured using a colorimetric assay using 6.5 mM L-alanine-4-nitroanilide. Each data point represents the means $\pm$ S.D. of eight to ten individual time-courses for each experimental condition.

[1] To whom correspondence should be addressed (email stefan.broer@anu.edu.au)

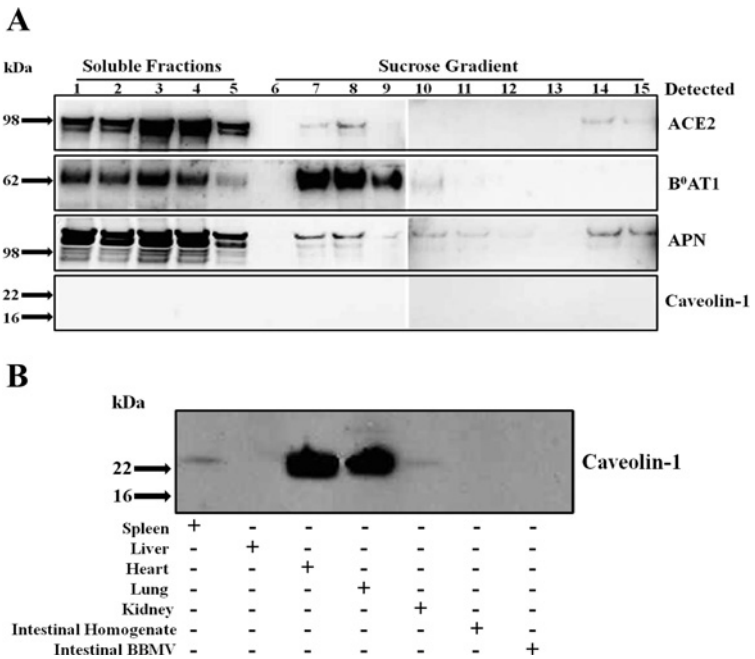

Figure S2 Isolation of detergent-resistant membranes from BBMV

(**A**) BBMVs (2 ml at 1–2 mg/ml) were treated with 1 % (v/v) Triton X-100 at 0–4 °C and centrifuged in a linear sucrose gradient for 24 h. All fractions were analysed by SDS/PAGE. Following semi-dry transfer on to a nitrocellulose membrane, individual proteins were visualized using immunoblot analysis as indicated next to each blot. Sucrose gradient fractions (1 ml) are numbered from highest to lowest density, 1 to 15, respectively ($e = 4$). (**B**) Tissue samples were homogenized at a concentration of 50 mg/ml and 20 μg/sample was loaded on to the gel and subjected to SDS/PAGE. Caveolin-1 was visualized using immunoblot analysis. Molecular masses are indicated to the left-hand side in kDa.

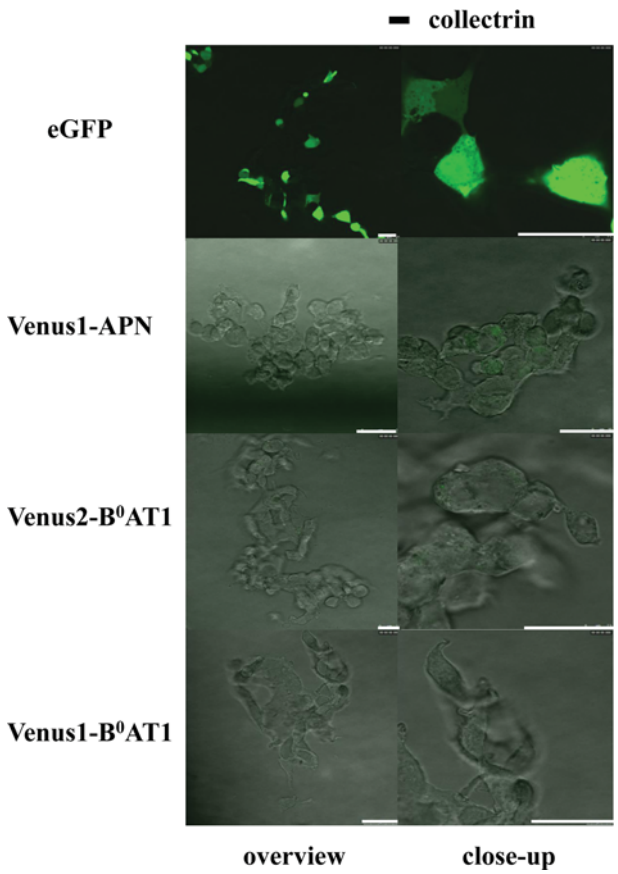

Figure S3 Co-localization of B0AT1 and APN

HEK-293 cells were transfected with 1.6 μg of plasmid DNA (constructs used are indicated to the left-hand side) approximately 48 h after seeding into eight-well microscope slide dishes, when cells had achieved >90 % confluency. The eGFP fluoresence was visualized with a Leica SP5 confocal system and processed with LAS AF software. The white scale bar indicates 25 μm. All images were taken at $\times$63 magnification.

Received 17 February 2012/23 May 2012; accepted 7 June 2012
Published as BJ Immediate Publication 7 June 2012, doi:10.1042/BJ20120307

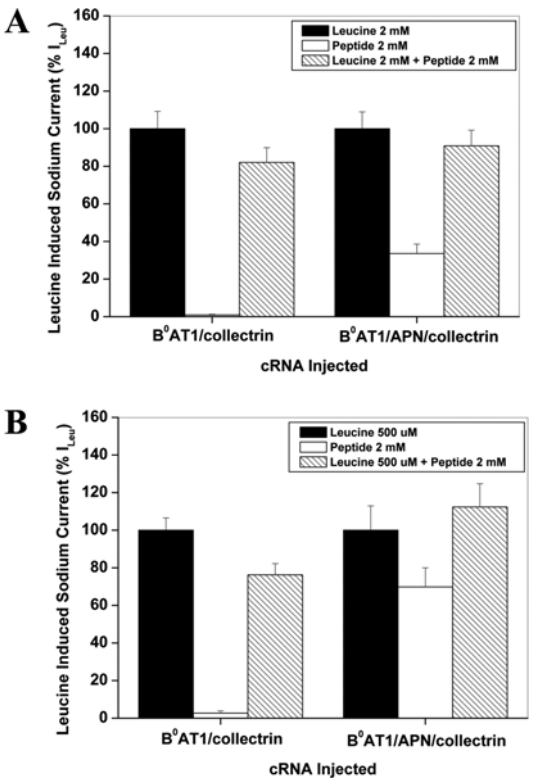

Figure S4 Mechanism of APN-mediated increase in substrate affinity

Oocytes were injected with 10 ng of B^0AT1 cRNA, 15 ng of APN cRNA and 2 ng of collectrin cRNA. (**A**) Oocytes were voltage clamped at -50 mV and subsequently superfused with either 2 mM leucine or 2 mM leucine tripeptide. All Na^+ currents were normalized to the sodium currents elicited by 2 mM leucine (I_{Leu}) at 100 %. Each bar represents the mean $\pm$ S.D. ($n = 15$). (**B**) Oocytes were recorded and superfused as indicated in (**A**), but using a leucine concentration of 0.5 mM. All Na^+ currents were normalized to the sodium currents elicited by 0.5 mM leucine (I_{Leu}) at 100 %. Each bar represents the mean $\pm$ S.D. ($n = 14$).